



**HAL**  
open science

# Convergent evolution of water-conducting cells in *Marchantia* recruited the ZHOUPI gene promoting cell wall reinforcement and programmed cell death

Yen-Ting Lu, Jeanne Loue-Manifel, Norbert Bollier, Philippe Gadiant, Freya de Winter, Philip Carella, Antoine Hoguein, Shona Grey-Switzman, Hugo Marnas, Francois Simon, et al.

## ► To cite this version:

Yen-Ting Lu, Jeanne Loue-Manifel, Norbert Bollier, Philippe Gadiant, Freya de Winter, et al.. Convergent evolution of water-conducting cells in *Marchantia* recruited the ZHOUPI gene promoting cell wall reinforcement and programmed cell death. *Current Biology - CB*, 2024, 34 (4), pp.793-807. 10.1016/j.cub.2024.01.014 . hal-04434325

**HAL Id: hal-04434325**

**<https://hal.science/hal-04434325v1>**

Submitted on 16 Oct 2024

**HAL** is a multi-disciplinary open access archive for the deposit and dissemination of scientific research documents, whether they are published or not. The documents may come from teaching and research institutions in France or abroad, or from public or private research centers.

L'archive ouverte pluridisciplinaire **HAL**, est destinée au dépôt et à la diffusion de documents scientifiques de niveau recherche, publiés ou non, émanant des établissements d'enseignement et de recherche français ou étrangers, des laboratoires publics ou privés.

1 **Convergent evolution of water conducting cells in *Marchantia***  
2 ***polymorpha* by recruitment of the *ZHOUP1* regulatory module**  
3 **promoting programmed cell death**

4  
5  
6 Yen-Ting Lu<sup>1¶</sup>, Jeanne Loue-Manifel<sup>1,2¶</sup>, Norbert Bollier<sup>3</sup>, Philippe Gadiant<sup>1</sup>, Freya De Winter<sup>3</sup>,  
7 Philip Carella<sup>4</sup>, Antoine Huguin<sup>1</sup>, Shona Grey-Switzman<sup>1</sup>, Hugo Marnas<sup>1</sup>, Francois Simon<sup>1</sup>,  
8 Alice Copin<sup>1</sup>, Shelby Fischer<sup>1</sup>, Erica de Leau<sup>1</sup>, Sebastian Schornack<sup>4</sup>, Ryuichi Nishihama<sup>5,6</sup>,  
9 Takayuki Kohchi<sup>5</sup>, Nathalie Depège Fargeix<sup>2</sup>, Gwyneth Ingram<sup>2</sup>, Moritz K. Nowack<sup>3,7\*</sup> and  
10 Justin Goodrich<sup>1,8\*</sup>

11  
12 ¶ These authors contributed equally to this work

13 \* Correspondence: [Moritz.Nowack@psb.vib-ugent.be](mailto:Moritz.Nowack@psb.vib-ugent.be), [Justin.Goodrich@ed.ac.uk](mailto:Justin.Goodrich@ed.ac.uk)

14  
15 <sup>1</sup>Institute of Molecular Plant Science, University of Edinburgh, Max Born Crescent, Edinburgh  
16 EH9 3BF, UK.

17 <sup>2</sup>Laboratoire Reproduction et Développement des Plantes, University of Lyon, ENS de Lyon,  
18 UCB Lyon 1, CNRS, INRAE, F-69342, Lyon, France.

19 <sup>3</sup>Center for Plant Systems Biology, VIB, Ghent 9052, Belgium.

20 <sup>4</sup>Sainsbury Laboratory, University of Cambridge, Bateman Street, Cambridge CB2 1LR, UK.

21 <sup>5</sup>Graduate School of Biostudies, Kyoto University, Kyoto 606-8502, Japan.

22 <sup>6</sup>Department of Applied Biological Science, Faculty of Science and Technology, Tokyo  
23 University of Science, Noda 278-8510, Japan.

24 <sup>7</sup>Department of Plant Biotechnology and Bioinformatics, Ghent University, Ghent 9052,  
25 Belgium

26 <sup>8</sup>Lead Contact

27 **Abstract**

28

29 A key adaptation of plants to life on land is the formation of water conducting cells (WCC) for  
30 efficient long-distance water transport. Based on morphological analyses it is thought that  
31 WCC have evolved independently on multiple occasions. For example, WCC have been lost  
32 in all but a few lineages of bryophytes but strikingly, within the liverworts, a derived group  
33 termed the complex thalloids has evolved a novel externalised water conducting tissue,  
34 composed of reinforced, hollow cells termed pegged rhizoids. Here we show that pegged  
35 rhizoid differentiation in *Marchantia polymorpha* is controlled by orthologues of the *ZHOUP1*  
36 and *ICE* bHLH transcription factors required for endosperm cell death in Arabidopsis seeds.  
37 By contrast, pegged rhizoid development was not affected by disruption of *MpNAC5*, the  
38 *Marchantia* orthologue of the *VND* genes that control WCC formation in flowering plants. We  
39 characterize the rapid, genetically controlled programmed cell death process that pegged  
40 rhizoids undergo to terminate cellular differentiation, and identify a corresponding  
41 upregulation of conserved putative plant cell death effector genes. Lastly, we show that  
42 ectopic expression of *MpZOU1* increases production of pegged rhizoids and enhances  
43 drought tolerance. Our results support that pegged rhizoids having evolved independently  
44 of other WCC. We suggest that elements of the genetic control of developmental cell death  
45 are conserved throughout land plants and that the *ZHOUP1/ICE* regulatory module has been  
46 independently recruited to promote cell wall modification and programmed cell death in  
47 liverwort rhizoids and in the endosperm of flowering plants.

## 48 Introduction

49

50 A striking and predictable feature of evolution is that traits are lost if there is no selective  
51 pressure to maintain them – well-known examples are the loss of sight in cave dwelling  
52 animals or the absence of chlorophyll in parasitic plants. This presents a problem if selection  
53 pressures change and it becomes advantageous to reacquire that trait, as the underlying  
54 genetic pathways may have been lost. One solution to this problem is to re-evolve the trait  
55 by modification of alternative gene networks (co-option), with the result that the final  
56 product invariably differs from the original. For example, monocots have lost the ability to  
57 make thick woody stems via secondary growth, but a few lineages such as *Yucca* have re-  
58 evolved an anomalous form of secondary growth (1). In most cases the accompanying genetic  
59 changes are not well understood. The evolution of water conducting tissues was a key  
60 adaptation to life on land in plants and is thought to have evolved multiple times  
61 independently, yet presents a tractable system as many of the genes directing WCC  
62 differentiation are known.

63 Extant land plants divide into two early diverging monophyletic groups, the  
64 bryophytes (hornworts, liverworts and mosses) and the tracheophytes (lycophytes, ferns,  
65 gymnosperms and angiosperms) (2). The tracheophytes possess an interconnected system of  
66 internal water conducting cells (WCC), tracheids or vessels, with the distinct features that  
67 they are elongated, have patterned cell wall reinforcement and undergo programmed cell  
68 death at maturity to produce hollow conduits devoid of cytoplasmic content to optimize  
69 water transport (3). Their WCCs are internal to plant organs and water can be transported  
70 over long distances by passing between individual cells via specialised cell-cell connections  
71 such as pit pairs in tracheids or perforation plates in vessels. The VASCULAR-RELATED NAC-  
72 DOMAIN (VND) family of transcription factors are master regulators of vessel differentiation  
73 in angiosperms, and are also strongly implicated in tracheid differentiation in gymnosperms  
74 (4-6). Although bryophytes are typically small and lack WCC, several basal and a few derived  
75 lineages in liverworts and mosses possess internal strands of interconnected WCCs that lack  
76 cytoplasmic content at maturity (7, 8). Because there is wide variation in cell wall  
77 composition, presence or absence of cell wall pores, and the way pores form it is thought that  
78 that the different types of WCC in bryophytes evolved independently from one another and

79 from those of tracheophytes (7, 9). Unexpectedly, the orthologues of the *VND* genes that  
80 control WCC development in tracheophytes were also found to control hydroid development  
81 in the model moss *Physcomitrium patens* (10). This suggests, instead, that the most recent  
82 common ancestor of land plants possessed a vascular system controlled by *VND* genes, and  
83 that this was subsequently lost or diversified in most bryophytes as a result of reduction in  
84 size and simplification of body plan.

85 Strikingly, within liverworts a derived group termed Marchantiopsida (complex  
86 thalloids) have evolved a novel water conducting system consisting of bundles of pegged  
87 rhizoids (11-14). Rhizoids are tip growing single cells that emerge from the lower (ventral)  
88 side of the liverwort body (thallus), similar to root hairs of vascular plants. In addition to  
89 regular, smooth, rhizoids, Marchantiopsida possess specialized pegged rhizoids that have  
90 have three characteristic features of WCC: they are highly elongated, possess cell wall  
91 reinforcements (called pegs), and are dead at maturity. Typically the pegged rhizoids collect  
92 together in bundles covered by scales to form pseudo-vascular bundles along the ventral  
93 midrib of thallus (12, 14), although some grow down into the soil substrate. However, they  
94 differ from vascular WCC by being exgternal, tip-growing individual cells that are separate  
95 from one another, i.e. their cell walls are not cemented together.

96 Consistent with pegged rhizoids originating independently of other WCC, we found  
97 that two transcription factors unrelated to *VND* genes control WCC differentiation in  
98 Marchantia, namely orthologues of the basic helix loop helix (bHLH) transcription factors  
99 ZHOUP1 (ZOU) and INDUCER OF CBF EXPRESSION1 (ICE1). By contrast, mutations in the  
100 Marchantia *VND* orthologue did not affect rhizoid development. In *Arabidopsis thaliana*, ZOU  
101 and ICE1 act as a heterodimer with various key roles during seed development, including  
102 promoting the cell death and elimination of endosperm and the formation of an intact  
103 embryonic cuticle (15-18). Both proteins are conserved throughout land plants (19, 20),  
104 raising the question of their ancestral role in plants lacking seed or endosperm. Our results  
105 suggest a conserved function in promoting cell death that has been independently recruited  
106 to diverse biological functions.

107

## 108 **Results**

109

110 **ZOU and ICE genes are conserved in land plants**

111

112 To investigate the function of ZOU and ICE1 orthologs in bryophytes, we characterised  
113 their orthologues in the model liverwort *Marchantia polymorpha* (hereafter *Marchantia*).  
114 Phylogenetic analysis indicates that *Marchantia* has a single orthologue of *Arabidopsis* ZOU,  
115 MpbHLH38 (*Mp4g19650*) here designated MpZOU1 and a second paralogous gene  
116 MpZOU2/MpbHLH24 (*Mp8g04130*) that derives from an ancient duplication likely present in  
117 the common ancestor of land plants (Figure 1A). Two regions are conserved between the  
118 proteins (Figure 1B), the bHLH domain and a C-terminal protein interaction domain, termed  
119 ACT-Like (ACTL) (21, 22). The position of the two introns in the *Marchantia* and *Arabidopsis*  
120 ZOU genes is also conserved, consistent with their having a common evolutionary origin  
121 (Figure 1C and 1D). The two *Marchantia* co-orthologues of the *Arabidopsis* ICE genes,  
122 MpICE1/MpbHLH16 (*Mp4g04910*) and MpICE2/MpbHLH17 (*Mp4g04920*) which derive from  
123 a more recent duplication (Figure 1A), after the divergence of liverworts and mosses, were  
124 described previously (23). Although we could identify several algal bHLH proteins which also  
125 had ACTL domains, our phylogenetic analysis (Figure 1A) showed that they were not  
126 orthologous with ZOU or ICE proteins and is consistent with other phylogenetic studies of  
127 land plant bHLH proteins (19, 20, 24).

128 We first tested whether the *Marchantia* ZOU and ICE proteins could interact with one  
129 another using a yeast two hybrid assay. Indeed, MpZOU1 and MpICE1 interact both with each  
130 other, and also with *Arabidopsis* AtICE1 and AtZOU, respectively (Figure 2A, 2B and 2C).  
131 Further, the full-length ICE proteins had transcriptional activation activity in yeast (Figure 2B)  
132 and a C-terminal portion that included the bHLH and ACTL domains was sufficient for  
133 interaction with ZOU proteins (Figure 2C). We next tested whether the *Marchantia* genes  
134 could rescue the seed phenotypes of their corresponding *Arabidopsis* mutants when  
135 expressed in transgenic seed from the *Arabidopsis* ZOU or ICE promoters. The seed of *Atzou*  
136 and *Atice1* mutants contains a small embryo which does not fill the seed, due to the presence  
137 of a persistent endosperm which impedes embryo growth. In addition, the seed is shrivelled,  
138 due to the collapse of the watery endosperm cells during seed maturation and desiccation  
139 (17). In *Atzou-4* mutants, expression of either the AtZOU or MpZOU1 coding sequences from  
140 the AtZOU promoter gave a full rescue, with a large embryo filling the oval shaped seed and  
141 no shrivelling (Figure 2D and 2E). In *Atice1-2* mutants, expression of AtICE1 gave a full rescue,

142 whereas *MpICE1* gave a partial rescue such that many seed had larger embryos and less  
143 shrivelling than in *ice1-2* but were misshapen relative to wild type (Figure 2D and 2E).  
144 Furthermore, both *MpZOU1* and *MpICE1* rescued the cuticle defects of *zou-4* and *ice1-2*  
145 mutants as measured by toluidine blue staining of etiolated seedlings (Figure 2F and 2G).  
146 Collectively these data support that the ZOU ICE partnership arose early in land plant  
147 evolution and the properties of the proteins have been broadly conserved in bryophyte and  
148 angiosperm lineages that diverged about 430 million years ago.

149

### 150 ***MpZOU1* and *MpICE1* promote pegged rhizoid differentiation**

151

152 To determine the developmental function of *MpZOU1* and *MpICE1* in *Marchantia*, we first  
153 examined their expression using transcriptional reporters comprising 5 and 6.6kb of  
154 regulatory sequences upstream of the start codons, respectively, fused either to the *GUS*  
155 gene encoding  $\beta$ -glucuronidase. The *proMpZOU1:GUS* and *proMpICE1:GUS* reporters were  
156 expressed strongly in 20 day old thallus tissue and with similar patterns, in ventral tissues  
157 around the midrib (Figure 3A-3F). In sections of gemma cups both genes were expressed in  
158 developing gemmae in the rhizoid initials, distinctive large, round cells that differentiate  
159 directly within the epidermis. (25) (Figure 3G and 3H). Following gemma germination,  
160 rhizoids and ventral scales are initiated near the apical notch (meristem) from its ventral  
161 cell derivatives (26). Both reporters were expressed at the apical notch, and in the rhizoid  
162 initials and emerging tubular rhizoids behind the notch (Figure 3I-J, L-M). In transverse  
163 sections of wax embedded tissues the *MpZOU1* reporter was expressed in ventral  
164 parenchyma and in the young scales surrounding the midrib (Figure 3K). The *MpICE1*  
165 reporter had similar expression ventrally but was little expressed in scales and also showed  
166 weak expression dorsally in the air chambers. Both reporters were expressed at the notch  
167 and in emerging scales, with *MpZOU1* confined to ventral tissues whereas *MpICE1* was  
168 expressed more broadly, dorsally and ventrally (Figure 3 O-Q). We also examined nuclear  
169 localized TdTomato reporter expression (*proMpZOU1:NLS-TdTomato* and *proMpICE1:-NLS-*  
170 *TdTomato*) in two-week old thalli and observed nuclear reporter signals in the thallus and in  
171 emerging and growing rhizoids (Figure S1 A-B). Imaging of rhizoid tips revealed expression in  
172 all rhizoids. These included both differentiating pegged rhizoids and rhizoids without visible  
173 pegs, i.e. smooth rhizoids or incipient, not yet fully differentiated pegged rhizoids (Figure S1

174 C-D). In conclusion these results suggested a role for *MpZOU1* and *MpICE1* in rhizoid  
175 development as both reporters were co-expressed in rhizoids from their initiation onwards.  
176 The reporters were broadly expressed in rhizoids, i.e. not obviously restricted to incipient  
177 pegged or smooth rhizoids. At least in *Arabidopsis* it is well documented that the activity  
178 and stability of ICE proteins is post-translationally regulated (27), so transcription licences  
179 but does not guarantee activity .

180 To see whether the expression in rhizoids was functionally relevant, we created  
181 multiple independent loss of function alleles of *MpZOU1* using genome editing to create  
182 frameshift mutations in the region encoding the bHLH domains (Figure S2 A-C). The alleles  
183 are likely to be null as they are predicted to cause premature termination of translation,  
184 truncating the proteins and removing the conserved bHLH and ACTL domains. We first  
185 examined whole mount, cleared thallus tissue of 12 day old plants using differential  
186 interference contrast microscopy, as this allowed us to check large number of rhizoids. Wild  
187 type plants had a mixture of smooth and pegged rhizoids, whereas the mutants had smooth  
188 rhizoids but lacked pegged rhizoids (Fig. 4A and Table S1A). Smooth rhizoids are typically  
189 wider in diameter than pegged rhizoids (12, 14) and in the mutants the rhizoids had similar  
190 diameter as smooth ones (Table S1B). In thallus tissue of older plants the pegged rhizoids are  
191 arranged in bundles along the midrib on the ventral surface of the thallus and are covered by  
192 pigmented scales to form an externalised vein (Figure 4C). In transverse sections of the midrib  
193 of the thallus of 10 week old wild type and mutant plants, the mutants lacked pegged rhizoids  
194 in the midrib and instead smooth rhizoids were present (Figure S3A). Rarely, rhizoids with  
195 small, poorly developed pegs were produced in thallus and gametangiophores of mutants  
196 (see yellow arrows in Figure S3 A-B). Introduction of a transgene expressing the *MpZOU1*  
197 coding sequence (*proMpZOU1:MpZOU1 CDS*) into the *Mpzou1-1* mutant background restored  
198 pegged rhizoid formation, confirming that *MpZOU1* disruption caused the mutant phenotype  
199 (Figure 4A and Table S1). We also over-expressed *MpZOU1* (*proMpEF1:MpZOU1 CDS*,  
200 hereafter *MpZOU1-OE*) and observed that in young gemmae all rhizoids were pegged (Figure  
201 4A). As in wild-type plants these rhizoids were produced from the ventral but not the dorsal  
202 epidermis (Figure 4B). This differs from transgenic plants that mis-express (via viral CaMV 35S  
203 enhancers) the *ROOT HAIR SIX-LIKE1* class bHLH gene *MpRSL1* required for rhizoid cell  
204 formation, as in these plants rhizoids are produced ectopically from the dorsal epidermis as  
205 well as ventrally (28). In wild type plants grown under far red enriched light, the thallus grow



206 upwards away from the soil and smooth rhizoids emerge in rows parallel to the midrib,  
207 external to the scales and grow perpendicular to the thallus form an aerial “beard” (Figure  
208 4C). In MpZOU1-OE, where present this “beard” consisted of pegged rhizoids, suggesting  
209 both that the growth of pegged rhizoids parallel to the thallus is due to constraint by overlying  
210 scales, and that MpZOU1 overexpression causes smooth rhizoids to differentiate as pegged.  
211 Consistent with this, in transverse sections of MpZOU1-OE rhizoids, we did not observe the  
212 wider, lighter staining ones characteristic of smooth rhizoids (Figure 4C) and these  
213 differences in rhizoid diameters were statistically significant (Table S1B). We also performed  
214 genome editing of MpICE1 and identified independent mutant alleles (Figures 4E and S1D –  
215 S1F). The Mpice1 mutants had a very similar phenotype to Mpzou1 (Figures 4E and S2A), but  
216 unlike MpZOU1, over-expression of MpICE1 did not cause smooth rhizoids to develop as  
217 pegged. Introducing MpICE1-OE into Mpice1 mutants complemented the mutant phenotype,  
218 confirming the functionality of the transgene (Figure 4D). Lastly, when we introduced  
219 MpZOU1 OE into the Mpice1 mutant background all rhizoids remained smooth (Figure 4D),  
220 indicating that MpICE1 is necessary for MpZOU1 activity. Collectively these data indicate that  
221 MpZOU1 and MpICE1 act together as a heterodimer with MpZOU1 giving specificity to or  
222 limiting the activity of the heterodimer. We suggest that the formation of rhizoid primordia  
223 is specified by MpRSL1, and MpZOU1/MpICE1 promote their differentiation as pegged  
224 rhizoids.

225

## 226 **MpZOU1 and MpICE1 regulate cell death and cell wall modification genes**

227

228 To identify genes acting downstream of MpZOU1/MpICE1 as effectors of pegged  
229 rhizoid differentiation, we carried out transcriptional profiling (RNAseq) of 12 day old  
230 gemmae of wild type, Mpzou1 and Mpice1 mutants. Since MpICE1 activated transcription in  
231 yeast assays (Figure 2B), and co-expression of ZOU and ICE genes activates transcription in  
232 several *in planta* assays in moss and tobacco (15, 29), we looked for transcripts that were less  
233 abundant in mutants compared to wild type. Consistent with their shared phenotype, a large  
234 and statistically significant fraction of the down regulated genes were common to the two  
235 mutants (Figure 5A and Data S2). Strikingly, within this shared set of 119 genes, we identified  
236 numerous genes linked with developmental programmed cell death (dPCD) in xylem or other  
237 cell types (Table S2). For example, MpMCA-Ilc (Mp8g07700) encoding a type II metacaspase

238 (see Data S1B for phylogeny) was strongly downregulated. In Arabidopsis there are six type II  
239 metacaspases (MC4-9), cysteine proteases with various roles in cell death and immunity (30,  
240 31) including Metacaspase9 (MC9) associated with cell death during xylem differentiation  
241 (32). In addition, five genes encoding DUF679 Domain Membrane proteins (DMP) were down  
242 regulated (Data S1C for phylogeny). Arabidopsis encodes ten DMP proteins including DMP4  
243 whose expression is tightly associated with various developmental programmed cell death  
244 (dPCD) processes including xylem differentiation and endosperm breakdown (32, 33). Six  
245 aspartyl proteases were downregulated and were orthologous to the rice aspartyl protease  
246 OsAP37 involved in tapetal dPCD (34)(Data S1D for phylogeny) . Numerous genes involved in  
247 cell wall modification and potentially linked to peg production or tip growth were found  
248 including several predicted rhamnogalacturonan endolyases and xyloglucan  
249 endotransglycosylases (Table S2). The dataset was also strikingly enriched for peroxidases,  
250 with 17 downregulated, of which 16 are predicted to be class III, i.e. secreted and apoplastic.  
251 Class III peroxidases have various roles, and are often associated with cell wall remodelling,  
252 including the polymerisation and crosslinking of phenolic units to form lignins and suberin  
253 (35). Although bryophytes lack lignin, it is possible that the pegs are reinforced via phenolic  
254 crosslinking, alternatively the peroxidases could be involved in ROS generation that enters  
255 the cell via aquaporins and triggers dPCD. Notably we did not find upregulation of *MpNAC5*  
256 (*Mp6g20920*), the single Marchantia orthologue of the *VND* genes that control differentiation  
257 of WCC in mosses and tracheophytes (see phylogeny in Data S1A and also in 10, 36). In  
258 addition, *Mpnac5* mutants had normal pegged rhizoid formation (Figure S4). Thus *MpNAC5*  
259 does not affect pegged rhizoid formation, although we can not exclude that redundancy with  
260 other NAC encoding genes masks the loss of function phenotype. Indeed, in Arabidopsis  
261 endosperm several (non *VND*) NAC genes including *KIRA1*, *SOMBRERO* and *ORESARA1*  
262 redundantly promote cell death, although *AtZOU/AtICE1* play the major role (18).

263 To confirm that the dPCD associated genes identified in RNAseq and/or scRNAseq  
264 were expressed during pegged rhizoid differentiation we made reporter lines for the  
265 metacaspase (*proMpMCA-IIc:tdTomato-NLS*) and for the DMP4/DUF679 gene *MpDMP1*  
266 (*Mp4g17600*) (*proMpDMP1:tdTomato-NLS*) using 2kb of sequences upstream of the ATG start  
267 codons. In several independent lines, 2-week old plants showed strong nuclear-localized  
268 tdTomato signals specifically in rhizoids and particularly in pegged-rhizoids (Figure 5B-C). To  
269 test whether *MpZOU1* regulated the activity of the reporters, we introduced them into

270 mutant and overexpression (OE) lines via gemma transformation. In 6-week old plants  
271 *Mpzou1* plants in which pegged-rhizoid differentiation is impaired almost no tdTomato signal  
272 could be observed (Figure 5D-F). Conversely in the MpZOU1 OE lines many rhizoids showed a  
273 strong tdTomato signal (Figure 5D-F). Quantification of the number of rhizoids showing  
274 nuclear tdTomato in 6-week old plants revealed an increased and decreased number in the  
275 *MpZOU1* OE and *Mpzou1* mutants relative to wild type, respectively, in accordance with the  
276 previously observed increased and decreased number of pegged-rhizoids in these genotypes  
277 (Figure 5G). Together our results indicate that MpZOU1 promotes expression of orthologues  
278 of established dPCD-associated genes during pegged rhizoid differentiation, either directly or  
279 indirectly.

280

### 281 **Pegged rhizoids undergo programmed cell death as a terminal differentiation step**

282

283 Next, we asked whether the differential regulation of PCD-associated gene  
284 orthologues in *Mpzou1* mutants and MpZOU1-OE lines caused less or more dead rhizoids.  
285 First, we imaged rhizoids of 19-day old thalli stained with the live-stain fluorescein diacetate  
286 (FDA) and the cell-wall stain propidium iodide (PI). In *Mpzou1-1* we could not detect dead  
287 (FDA-negative, PI-positive) rhizoids, and in MpZOU1-OE there were visibly more dead rhizoids  
288 when compared to wild type (Figure 5H-J). To quantify this effect, we imaged wild type,  
289 *Mpzou1* mutants and MpZOU1-OE lines expressing nuclear localized mTurquoise and plasma  
290 membrane (PM) localized mScarlet-I (*proMpUBE2:mTurquoise-N7*, *proMpUBE2:ScarletI-Lti6b*)  
291 (Figure S5). Counting nuclear foci in 19-day old thalli revealed a slight non-significant increase  
292 of nuclei in *Mpzou1-1*, and a significant decrease of nuclei in MpZOU1-OE in comparison with  
293 wild type (Figures 5K and S4). Though it is impracticable to determine the total number of  
294 rhizoids, and therefore to determine the ratio of living to dead rhizoids, these numbers  
295 suggest that MpZOU1 promotes not only the formation of rhizoidal pegs but also the  
296 execution of a cell death program in rhizoids.

297 To characterize the execution of differentiation-induced cell death in rhizoids in more  
298 detail, we performed live-cell imaging of rhizoids expressing the *proMpUBE2:mTurquoise-N7*,  
299 *proMpUBE2:ScarletI-Lti6b* double reporter construct. Imaging revealed that arrest of tip  
300 growth was the earliest sign of terminal differentiation: While smooth rhizoids grew fast,  
301 differentiating pegged rhizoids arrested growth (Video S1). Next, imaging of the

302 *proMpZOU1:NLS-tdTomato* reporter line in wild-type showed that peg formation proceeded  
303 gradually toward the rhizoid tip, reaching it before cell death execution (Figure 6A and Video  
304 S2). Detailed analysis of the *proMpUBE2:mTurquoise-N7*, *proMpUBE2:Scarlet1-Lti6b* double  
305 reporter construct revealed successive discrete steps of cell death execution: First the  
306 integrity of the nuclear envelope was compromised, leading to a leakage of the *mTurquoise-*  
307 *N7* reporter into the cytosol (Figure 6B, cyan arrowheads, and Video S1). Next, the *Scarlet1-*  
308 *Lti6b* signal dissociated from the plasma membrane and became freely soluble in the cytosol  
309 (Figure 6B, magenta arrowhead, Video S1). After this step, the tonoplast ruptured, indicated  
310 by an even distribution of the Scarlet1 signal in the entire cell lumen (Figure 6B, white  
311 arrowhead, Video S1). As a final step, the plasma membrane integrity was lost, leading to a  
312 diffusion of the Scarlet signal into the apoplastic extracellular space (Figure 6B, yellow  
313 arrowhead, Video S1). Collectively these data support that pegged rhizoid differentiation  
314 involves a rapid, genetically programmed execution with typical features of dPCD including  
315 nuclear rupture and vacuolar collapse.

316 Both cell wall reinforcement as well as programmed cell death are a typical feature of  
317 WCCs in tracheophytes. To visualize the solute flow into pegged rhizoids, we performed  
318 confocal time lapse imaging of fluorescein-stained rhizoids. Fluorescein is a fluorescent dye  
319 routinely used to visualize solute flow in plants (37), and is non-membrane permeable, thus  
320 being excluded from rhizoid cells as long as their plasma membrane is intact. Imaging of the  
321 *proMpZOU1:NLS-tdTomato* reporter line in wild-type showed that fluorescein entered the  
322 pegged rhizoid shortly after nuclear envelope breakdown (Figure 7A, red arrowhead, and  
323 Video S3). These data suggest that efficient passive water transport through the rhizoids  
324 commences upon programmed cell death in the pegged rhizoids.

325 To test if pegged rhizoids growing in the substrate are involved in water transport to  
326 the thallus, we subjected wild-type and *MpZOU1-OE* plants to a drought assay in soil. While  
327 well-watered thalli of wild type and *MpZOU1-OE* display a similar photosystem II (PSII)  
328 photochemical efficiency as indicated by the Fv/Fm ratio (38), thalli subjected to drought  
329 showed clear differences (Figure 7B, D). Drought-exposed wild type thalli were visibly wilted  
330 and displayed a strong reduction of PSII efficiency, whereas *MpZOU1-OE* thalli were visibly  
331 turgid and showed only a weak reduction in PSII photochemical efficiency (Figure 7C, D).  
332 These data indicate that *MpZOU1-OE* thalli were less affected by drought. Though we cannot  
333 exclude that other effects of *MpZOU1* over- and misexpression contributes to this drought

334 resistance phenotype, our results suggest that pegged rhizoids are important for soil to  
335 thallus water transport.

336 The presence of pegged rhizoids in liverworts is correlated with species in which the  
337 female sexual organs are elevated above the thallus on stalks, facilitating spore dispersal via  
338 wind after fertilisation (12, 39). In *Marchantia*, two grooves run up the stalk and are densely  
339 packed with pegged rhizoids which have become partially internalised by inrolling of the  
340 thallus. Dye uptake experiments show that water passes up the stalk within these grooves  
341 (12, 26). In the stalks of *Mpzou1* and *Mpice1* mutants, transverse sections showed that  
342 normal pegged rhizoids were absent from the grooves and instead smooth rhizoids lacking  
343 pegs and larger in diameter were present (Figure 7E). Occasionally rhizoids developed pegs,  
344 but these were smaller and extended less far into the lumen of the rhizoid, suggesting that  
345 they were not fully differentiated (Figure S3B). Strikingly, the gametangiophores of mutants  
346 were typically smaller and less well differentiated than wild type and did not survive for long,  
347 shrivelling and drying out even when grown in enclosed, vented containers (i.e. with high  
348 humidity and no air currents) (Figure 7E). Possibly as a result the mutants were not fertile  
349 either as males or females. These results are consistent with the presence of pegged rhizoids  
350 in stalks being important for hydration and viability of the aerial gametangiophores.

351

## 352 Discussion

353

354 Pegged rhizoids possess the three defining features of WCC, namely that they are  
355 elongated tubular cells, with structural reinforcement of their cell walls and devoid of  
356 cytoplasmic content at maturity. Despite this, they have obvious differences from tracheary  
357 elements. Firstly, they are external to the plant epidermis, although partially internalised  
358 along the thallus' midribs and in the grooves in gametangiophore stalks. Secondly, they are  
359 unicellular tip growing protuberances so their cell walls are not cemented together by middle  
360 lamellae, precluding formation of intercellular connections such as pit pairs to allow water to  
361 pass from one cell to another. Instead, water passes up the entire furrow formed by the  
362 overlying scales and bundles of pegged rhizoids by capillarity (i.e. between as well as within  
363 rhizoids) and individual pegged rhizoids can take up this external water (12, 14). Current  
364 evidence suggests that the most recent common ancestor of land plants possessed an internal

365 vascular system regulated by *VND* genes which has been retained in a few early diverging  
366 mosses and liverworts lineages but was subsequently lost consistent with reduction in size,  
367 simplification of body plan and large scale gene loss (3, 7, 10, 40). Consistent with their  
368 distinctive features, phylogenetic analysis indicates that pegged rhizoids are a derived feature  
369 in liverworts, being absent in basal lineages such as Haplomitriopsida and within the  
370 Marchantiopsida (complex thalloids) they are not found in early diverging *Blasia* (39). The  
371 occurrence of pegged rhizoids has been correlated with species in which the archegoniophore  
372 is elevated (12), facilitating spore dispersal from multiple sporophytes on a single stalk.  
373 Consistent with an independent evolutionary origin of pegged rhizoids, their genetic control  
374 is distinctive. Unlike hydroids of mosses, their differentiation does not require *VND* gene  
375 activity but rather a separate regulatory module, *ZOU/ICE1*, which is also conserved in all land  
376 plants. In *Arabidopsis* the *ZOU/ICE* heterodimer controls dPCD and cell wall modification  
377 during endosperm differentiation. *ZOU/ICE* promotes expression of genes encoding cell wall  
378 modifying enzymes, leading to a softening of endosperm cells which allows the embryo to  
379 expand. This may act as a mechanical trigger for endosperm dPCD, which is orchestrated by  
380 both *ZOU/ICE* and *NAC* transcription factors (18) and marked by expression of canonical dPCD  
381 markers such as *DMP4* and aspartic proteases (16, 32). Despite the obvious differences  
382 between endosperm and rhizoids, the role of *ZOU1* in promoting dPCD across the large  
383 evolutionary distances between *Marchantia* and *Arabidopsis* is intriguing. However,  
384 independent of its transcriptional regulation, our results show that the process of dPCD is  
385 conserved throughout land plants and is characterized by the expression of conserved  
386 putative effectors such as metacaspases and DMP-related genes (32). In the future, single-  
387 cell RNA sequencing of differentiating pegged rhizoids might reveal more transcriptional  
388 similarities. Interestingly, the cell death execution in terminally differentiating pegged  
389 rhizoids shows many parallels to the sequence of cell death events that were recently  
390 described in *Arabidopsis* root cap cells undergoing developmentally controlled programmed  
391 cell death (41). In both *Marchantia* and *Arabidopsis*, nuclear envelope breakdown and  
392 solubilization of plasma membrane markers represent an early event in cell death execution,  
393 followed by collapse of the large central vacuole and permeabilization of the plasma  
394 membrane. This succession of events opens the possibility that developmentally controlled  
395 cell death execution is evolutionary conserved in land plants. The existence of several dPCD-  
396 associated gene orthologues throughout land plants (32) as well as the expression of

397 metacaspase and DMP orthologues in dying Marchantia rhizoids would be in line with this  
398 assumption. However, until there is more knowledge on the function of dPCD-associated  
399 genes, this discussion remains speculative.

400 Interestingly, while the plasma membrane remains impermeable for fluorescent  
401 proteins for several hours after cell death execution in Arabidopsis root cap cells (41),  
402 fluorescent proteins leak out from Marchantia rhizoids directly after vacuolar collapse.  
403 Possibly, the release of hydrolytic enzymes responsible for corpse clearance that would  
404 damage neighbouring root epidermis cells of the Arabidopsis root cap does not need to be  
405 controlled in Marchantia as rhizoids are not in close contact with other cells.

406 In conclusion, our results suggests that the ZOU/ICE partnership evolved in early land  
407 plants and had an ancestral function in promoting dPCD in the gametophyte. Given that the  
408 pegged rhizoids are a derived feature specific to the complex thalloid liverworts it will be  
409 interesting to know whether ZOU/ICE regulate other cell differentiation events involving  
410 dPCD in bryophytes. In maize and Arabidopsis *ZOU* expression is very specifically expressed  
411 in the endosperm (17, 29, 42) and not in sporophytic tissues (embryo, seedling, adult plant  
412 etc). This is intriguing as the endosperm has long been suggested to be the sexualised  
413 derivative of the haploid megagametophyte of gymnosperms and lycophytes (43). An  
414 attractive hypothesis is therefore that during land plant evolution, as the gametophyte  
415 became smaller and dependent on the maternal sporophyte the role of ZOU/ICE in dPCD and  
416 cell wall softening was retained to aid the breakdown of the maternal gametophyte tissue  
417 surrounding the developing embryos. Although lycophytes and gymnosperms lack  
418 endosperm, the growing embryo similarly invades surrounding nutritive maternal  
419 gametophytic tissue, for example the prothallium in gymnosperms. Indeed, a recent  
420 transcriptomic study indicates that *ZOU* orthologues are expressed in the megagametophyte  
421 of the gymnosperm *Pinus pinaster* (44). This role of ZOU/ICE role may have been retained in  
422 the angiosperm seed but restricted to the post fertilisation development of the endosperm.

423

## 424 **Materials and Methods**

425

### 426 **Plant Growth**

427

428 Wild type *Marchantia polymorpha* plants were Takaragaike-1 (Tak-1) males and  
429 Takaragaike-2 (Tak-2) females (Ishizaki et al., 2008). Plants were asexually maintained and  
430 propagated through gemmae growth on 100 X 100 X 20 mm square Petri dishes (Sarstedt  
431 82.9923.422) containing 1.4% agar (Sigma A9799) in 1 X Johnson's medium as described in  
432 (45, 46). Plants were grown under cool white fluorescent light (Philips TL-D/830 tubes) at  
433 approximately 120  $\mu\text{mol}/\text{m}^2/\text{s}$  intensity in long days (16 hour light:8 hours dark) at 22°C. To  
434 induce reproductive growth, three week old plants were transferred to soil (a 1:1 mixture of  
435 perlite and John Innes Compost no. 2) in tissue culture micropropagators equipped with  
436 microfilters for gas exchange (Duchefa OS140) and grown in long days under cool white  
437 fluorescent light supplemented with 730 nm far red light from a HORTLILED Multi 120cm  
438 low output (40W) far red LED strip (Hortilux Schreder, The Netherlands) at approximately  
439 47.5  $\mu\text{mol}/\text{m}^2$ . The *Arabidopsis Atzou1-4* and *Atice1-2* lines were described previously (17,  
440 47).

441

### 442 **Phylogenetic analysis**

443

444 The *Arabidopsis* ZOU and ICE protein sequence were used for BLASTP and TBLASTN (48)  
445 searches to retrieve similar protein sequences from various databases as follows:  
446 Marpolbase (<https://marchantia.info/>) for *Marchantia polymorpha*, *Physcomitrella patens*,  
447 *Selaginella moellendorffii*, *Salvinia cucullata*, *Picea abies*, *Amborella trichopoda*, *Spiroglaea*  
448 *musciicola*, *Chara braunii* and *Klebsormidium nitens*; Phytozome ([https://phytozome-](https://phytozome-next.jgi.doe.gov/)  
449 [next.jgi.doe.gov/](https://phytozome-next.jgi.doe.gov/)) for *Aquilegia coerulea*, *Mimulus guttatus*, *Nymphaea colorata*, *Oryza*  
450 *sativa*; Onekp (<https://db.cngb.org/onekp/>) for *Anthoceros punctatus* and for 147  
451 streptophyte and chlorophyte algal species. The retrieved sequences were aligned using  
452 MAFFT implemented within the Geneious package (<https://www.geneious.com>) and AUTO  
453 algorithm and BLOSUM62 scoring matrix. The alignment was manually trimmed to include  
454 the bHLH and ACTL domains and then positions with >10% gaps were stripped using the  
455 mask alignment tool in Geneious. The phylogenetic trees were produced using the Mr Bayes  
456 program implemented on the CIPRES server (<https://www.phylo.org/>) with a mixed amino  
457 acid model, and substitution rates modelled using  $\text{inv}\gamma = 4$ . The trees were  
458 run for up to 8 million generations with 25% of trees discarded in the burn in phase.  
459 Convergence was defined as when the average split deviation frequency was less than or  
460 equal to 0.01. The output tree was imported and edited using Figtree  
461 (<http://tree.bio.ed.ac.uk/software/figtree/>).

462

### 463 **Drought assay and measuring of photosynthetic performance**

464

465 Gemmae were placed on Gamborg B5 medium and grown under continuous light for 19  
466 days. They were then transferred to individual pots filled with a defined amount of potting  
467 soil and supplemented with a defined amount of tap water. Pots were distributed randomly  
468 over 5 trays and placed in a growth chamber with continuous light (white-light LED strips  
469 from VALOYA [Finland], model L35-144 NS12) delivering about 2900 lux to the plants. A  
470 well-watered state was maintained by watering the individual pots with a pipette to



471 maintain a defined total pot weight. After 6 days, some pots were not watered anymore,  
472 causing a gradually increasing drought, as indicated by a reduction in total pot weight, while  
473 control pots continued to receive water. After 11 days after onset of drought, photos of the  
474 thalli were taken, and photosystem II (PSII) maximum efficiency (Fv/Fm) was measured with  
475 an Imaging-PAM M-Series chlorophyll fluorescence system (Heinz Walz, Effeltrich, Germany)  
476 as described before (38, 49). Fv and Fm denote variable fluorescence (ability of PSII to  
477 perform photochemistry) and maximal fluorescence (PSII centres closed), respectively, and  
478 the Fv/Fm ratio can be interpreted as a measure of plant stress levels due to environmental  
479 factors such as drought (50).

480

## 481 **Plasmid construction**

482

483 All primers are listed in an Excel sheet (Data S3). PCR amplifications were performed using  
484 KOD Xtreme Hot Start proofreading DNA Polymerase (Merck Millipore) and the Touchdown  
485 protocol provided by the manufacturers. The sequence of constructs was verified by Sanger  
486 sequencing (Edinburgh Genomics at University of Edinburgh) or Plasmidsaurus  
487 (<https://www.plasmidsaurus.com/>).

488

489 The cDNA of the coding sequences of MpZOU1 and MpICE1 were amplified from Tak2  
490 thallus cDNA using *attB* adapted primers and (Merck Millipore), and the products were  
491 cloned into pDONR221, pDONR207 or pDONR P2R-P3 Gateway entry vectors by BP clonase-  
492 mediated recombination (Thermo Fisher Scientific). Gateway entry clones of the coding  
493 sequences of AtICE1 and AtZOU were made in the same way using cDNA from Col-0 siliques  
494 containing seed around the heart stage of embryo development. The AtICE1 cDNA was  
495 cloned using pCR8 gateway adapted entry vector (Thermo Scientific).

496

497 For yeast two hybrid experiments, we used LR clonase-mediated recombination to  
498 transfer cDNA clones from our pDONR entry clones into Gateway adapted yeast two hybrid  
499 vectors pGADT7-DEST and pGBKT7-DEST (51) as in-frame fusions to GAL4 transcriptional  
500 activation or DNA binding domains, respectively.

501

502 For complementation of the Arabidopsis *zou-4* mutant phenotype, we amplified 4.5  
503 kb of genomic sequences upstream of the AtZOU start codon using *attB* adapted primers  
504 and cloned into pDONR207 using BP clonase. To generate the *proAtZOU::MpZOU1* and  
505 *proAtZOU::MpICE1* constructs we performed a multisite Gateway recombination using LR  
506 clonase, “empty” pENTR5'-MCS2 (containing a short multiple cloning site sequence),  
507 pDONR221-*proAtZOU*, the relevant pDONR P2R-P3 derived coding sequence entry clone and  
508 pK7m34GW (52) binary destination vector (providing NOS 3'-transcriptional terminator  
509 sequences).

510

511 For complementation of the Arabidopsis *ice1-2* mutant phenotype, we used a clone  
512 of the AtICE1 promoter region previously shown (47) to be sufficient to drive  
513 complementation of the *ice1* seed phenotype, inserted in the 5' multisite Gateway entry  
514 vector P4-P1R pDONR (15). We then performed multisite Gateway recombination using LR  
515 clonase, pDONR-5'-*proAtICE1*, the relevant pDONR221 derived coding sequence entry clone,  
516 and an “empty” 3'-multisite Gateway pENTR3'-MCS clone with the destination vector  
517 pK7m34GW.

518

519 For complementation of the *Mpzou1-1* mutant phenotype, the *proMpZOU1:MpZOU1*  
520 CDS construct was made by Gibson Assembly using the NEB Builder enzyme mix. We  
521 amplified a 5kb region of genomic DNA upstream of the *MpZOU1* start codon and fused this  
522 to the *MpZOU1* coding sequences amplified from our cDNA entry clone (see above) and the  
523 backbone of the binary vector pMpGWB301 (53) digested with HindIII and SacI (provides  
524 *NOS* gene transcriptional terminator).

525

526 For *MpZOU1* and *MpICE1* transcriptional reporter constructs, we amplified  
527 sequences 5 and 6.6kb upstream of the start codons, respectively, using Tak2 genomic DNA  
528 as template and cloned into pDONR221 Gateway entry vector by BP clonase-mediated  
529 recombination. The resulting entry clones were recombined into the destination vectors  
530 pMpGWB104 or pMpGWB116 (53) for *GUS* and *tdTomato-NLS* reporters, respectively.

531

532 The OpenPlant toolkit (Sauret-Güeto et al., 2020) and Golden Gate Loop Assembly  
533 was used to generate the *proMpUBE2:mTurquoise-N7* ; *proMpUBE2:Scarlet1-Lti6b* construct by  
534 digestion-ligation of the pCsA, L1\_CsR-Ck1, L1\_UBE2:mT-N7-Ck2, L1\_UBE2:mS-Lt-Ck3 and  
535 pCk4\_spacer building blocks using *SapI*.

536

537 To make the reporters for dPCD associated genes, the *proMp4g17600*, *proMp8g07700*,  
538 promoter sequences (2kb upstream of ATG start codon) were PCR amplified from genomic  
539 DNA and first cloned into the pDONR221 by Gateway BP clonase mediated recombination  
540 and then into the pMpGWB116 vector using LR Clonase.

541

#### 542 **Histochemical analysis of GUS activity**

543

544 Histochemical assays for GUS activity were performed according to (54) with some minor  
545 modifications. Briefly, after three 20 minute vacuum infiltrations with the GUS staining  
546 solution (50mM sodium phosphate buffer, pH 7.2, 0.5mM potassium-ferrocyanide, 0.5mM  
547 potassium-ferricyanide, 10mM EDTA, 0.01% Triton, 1mM 5-bromo-4-chloro-3-indolyl-Beta-  
548 glucuronic acid (Duchefa Biochemie, CAS number 114162-64-0), plants were incubated  
549 overnight at 37°C. They were then dehydrated by incubation in increasing concentrations of  
550 Ethanol (15%, 30%, 50%), for 20 minutes at each step at room temperature. Plants were  
551 then fixed in FAA fixative solution (3.7% formaldehyde, 5% acetic acid, 50% ethanol) for 45  
552 minutes under vacuum followed by either 2 hours at room temperature or overnight at 4°C.  
553 Dehydration steps to remove the chlorophyll were then performed by incubation in further  
554 increasing concentrations of ethanol (50%, 70%, 100%), for 20 minutes at each step at room  
555 temperature. Observations of GUS activity on whole mount samples were made using a  
556 Keyence VHX900F digital microscope. For observation of tissue sections, 15 to 20 day-old  
557 thallus tissue was harvested and placed in a small petri dish and 5% Phytigel (Sigma CAS :  
558 71010-52-1 ; P8169) at 50°-60°C was then poured onto the plants. The plate was then  
559 stored for 30 min to 1hour at 4°C to solidify before mounting onto the Leica VT1000 S  
560 Microtome. Approximately 10µm sections were cut and placed into 1%PBS solution before  
561 staining as described above. Observations of GUS activity were made using a Keyence  
562 VHX900F digital microscope.

563

#### 564 **Fluorescent protein reporter lines imaging**

565

566 For imaging plants were grown and maintained on 0.5× Gamborg media (Gamborg B5  
567 medium plus vitamins, Duchefa Biochemie G0210, pH 5.8) and 1.2% (w/v) agar (Plant Tissue  
568 culture grade No. 4, Neogen), under continuous light emitted by white fluorescent lamps  
569 (intensity of 120  $\mu\text{mol}/\text{m}^2/\text{s}$ ) at 22°C. For time-course confocal imaging, gemmae were  
570 grown in imaging chambers (Nunc™Lab-Tek™II) containing solid 0.5 × Gamborg medium for  
571 14 days before imaging the rhizoids growing along the cover glass forming the bottom of the  
572 chambers. Images were collected every six minutes for time lapse using an X20 lens. For  
573 the reporter lines or marker lines, mTurquoise, mScarletI and TdTomato fluorescent  
574 proteins were excited with 405, and 561nm lasers using either a Zeiss LSM 710 inverted  
575 confocal or a Zeiss LSM 880 upright confocal microscope equipped with a 10x/0.45 Plan-  
576 Aplanachromat objective. The fluorescence emissions were collected at 460-485 for  
577 mTurquoise-N7, and 570-600nm for TdTOMATO and ScarletI. Image processing and analyses  
578 were conducted using Fiji (55). The processed images from Fiji were cropped and assembled  
579 for figures in Inkscape (<http://inkscape.org>).

580 For fluorescein imaging, a 1 molar stock solution was made by dissolving  
581 3.76 g of fluorescein (Fluorescein sodium salt, CAS Number: 518-47-8, Sigma-Aldrich) in  
582 10ml of double-distilled water. A 1:1000 working solution was made with liquid 0.5×  
583 Gamborg medium and added to the imaging chamber and allowed to diffuse through the  
584 solid medium before imaging.

585 Counting the nuclear foci to estimate the number of living rhizoids was done by confocal tile  
586 scan with a maximally opened pinhole to record nuclear signals of all rhizoids growing along  
587 the cover glass bottom of an imaging chamber. Nuclear foci were automatically counted by  
588 the Particle Analysis tool in image J. Statistical analyses were performed using the  
589 GraphPad Prism software version 10.0 (GraphPad Software, San Diego, USA).

590

### 591 **Generation of mutants by CRISPR/Cas9 Genome editing**

592

593 Mutants were generated as described in (56). Briefly, to mutate *MpZOU1*, *MpICE1* and  
594 *MpNAC5* we designed sgRNA using CRISPRdirect (<https://crispr.dbcls.jp/>) (57). To minimise  
595 off-target effects we designed at least two different sgRNA for each gene and confirmed  
596 that each induced similar phenotypes. The oligonucleotides encoding the sgRNA were first  
597 cloned into pGE\_EN03 by ligation of *BsaI* digested vector with annealed complementary  
598 DNA oligonucleotides. The sgRNA constructs were then transferred into Cas9 containing  
599 Gateway adapted binary T DNA vectors pMpGEO10 and pMpGEO11 by LR clonase-mediated  
600 recombination. To make *Mpzou1* and *Mpice1* single mutants, the editing constructs were  
601 used for sporeling transformation, for *Mpnac5* mutants Tak1 thallus was transformed. To  
602 identify mutations, genomic DNA from primary (T1) transformants was extracted, regions  
603 flanking the sgRNA were amplified by PCR and subject to direct sequencing. In cases where  
604 the T1 plants had sequence alterations we propagated them asexually via gemmae,  
605 confirmed the presence of the mutation in G1 gemmae and analysed phenotypes in G2 and  
606 subsequent generations.

607

### 608 **Marchantia DNA extraction and genotyping**

609

610 To amplify small (<1kb) DNA fragments for genotyping plants, a 3 x 3 mm piece of thallus  
611 was excised and put in a microtube containing 2 metal beads in each tube and 100  $\mu\text{l}$  Buffer

612 A (100 mM Tris-HCl (pH9.5), 1 M KCl, 10 mM EDTA), then the tissues was ground shaking in  
613 a Tissuelyser mixer (Qiagen) for 1 minute at 30 beat/sec then incubated at 95°C for 10  
614 minutes and diluted by adding 400 µl water. A 1 µl aliquot was used as a template in PCR  
615 reactions using KAPA2G Robust DNA polymerase (Sigma Aldrich), which performed well with  
616 impure DNA templates. PCR products were sequenced directly using the Sanger sequencing  
617 facility at Edinburgh Genomics, University of Edinburgh.

618  
619 For amplification of larger fragments such as promoters, a cetyltrimethylammonium  
620 bromide (CTAB) DNA extraction method was used. Thallus tissue (1g) was frozen in liquid  
621 nitrogen and ground with pestle and mortar, 0.1g or polyvinylpyrrolidone (PVP) added, then  
622 the frozen powder was resuspended in 10 ml extraction buffer (100 mM Tris-HCl (pH 8.0),  
623 1.4 M NaCl, 20 mM EDTA (pH 8.0), 2% CTAB) with freshly added β-mercaptoethanol (12 µl),  
624 mixed by vortexing periodically and incubated at 65°C for one hour. To remove proteins  
625 and other contaminants, two extractions with 10ml of Chloroform:Isoamylalcohol (24:1)  
626 were performed. The DNA was precipitated by addition of an equal volume of isopropanol  
627 to the aqueous phase, recovered by centrifugation at 3500g for 10 minute. The DNA pellet  
628 washed in 70% ethanol and then resuspended in 400 µl TE buffer (10mM Tris pH 8.0 1mM  
629 EDTA) containing 100 µg/ml RNase A and incubated at room temperature for 30 minutes.  
630 Finally, 0.1 volume (40ul) of 3M sodium acetate pH 5.5 and 2.5 volumes ethanol were  
631 added, mixed by inverting and the mixture spun in a bench top microfuge at 6.5k for 5  
632 minutes, the pellet washed in 70% ethanol, air dried for five minutes and resuspended in  
633 100 µl TE.

634

### 635 **Plant Transformation**

636

637 Constructs were introduced into *Agrobacterium tumefaciens* strain GV3101 mp90 by  
638 electroporation. Sporeling transformation was used to generate *Mpzou1* and *Mpice1*  
639 mutants, and *MpZOU1* and *MpICE1* overexpression lines. *M. polymorpha* spores from Tak-  
640 2 x Tak-1 crosses, (approximately 5 sporangia per transformation) were sterilised for  
641 15minutes with 0.1% sodium dichloroisocyanurate (Sigma Aldrich 218928) solution, spun for  
642 1 minute at maximum speed in a microcentrifuge, resuspended in 500µL of water and  
643 grown 7 days into 50mL of OM51C (46) liquid media under 130 rpm agitation at 22°C, 16  
644 hours light. *Agrobacterium*-mediated transformation of 7 day-old sporelings was performed  
645 as previously described in (58). Resulting cells were incubated under 16 hours light, 22°C.  
646 Gemmae from the second generation were subjected to further analysis.

647

648 For complementation of *Mpzou1-1* mutants and for introduction of cell death  
649 reporter genes into Tak1, *Mpzou1-1* and *proEF1::MpZOU1* backgrounds thallus  
650 transformation was performed as described in (59). Transformants were selected on  
651 medium containing hygromycin (10 mg/L) or chlorsulfuron (0.5 µM) and cefotaxime (100  
652 mg/L) and the presence of the transgene was confirmed by PCR analysis on G1 gemmae.

653

654 For complementation of *Arabidopsis* mutants, *Atice1-2* and *Atzou-4* plants were  
655 transformed using floral dip transformation (60) and T3 seed (where the primary  
656 transformants are designated T1) was examined in progeny of T2 plants homozygous for the  
657 transgene.

658

659 **Differential Interference Contrast (DIC) Microscopy**

660

661 For whole mount observation of rhizoids, plants were grown on inverted plates so that  
662 rhizoids grew away from the agar into air, so as to minimise damage during transfer from  
663 agar to microscope slides. 12-day old thallus were placed between the slide and coverslip  
664 with a drop of chloral hydrate: glycerol (7:1) solution overnight and analysed using a Zeiss  
665 Axioimager 2 with (DIC).

666

667 **Histology using wax embedded thallus tissue**

668

669 Plants were grown on soil and slices (about 1 cm long, 2cm back from apex where midrib  
670 prominent) of thallus were cut with a razor blade and fixed overnight at 4°C in 4%  
671 paraformaldehyde 2% Glutaraldehyde in 1X PBS containing 10% DMSO, 0.1% Triton-X-100  
672 and 0.1% Tween-20 with 10 minutes gentle vacuum infiltration at onset. The fixed tissue  
673 was washed twice for ten minutes in 1 X phosphate buffered saline (PBS 7 mM Na<sub>2</sub>HPO<sub>4</sub>, 3  
674 mM NaH<sub>2</sub>PO<sub>4</sub>, 130 mM NaCl), transferred to 50% ethanol and subsequent dehydration and  
675 wax infiltration was performed using an automated processor (Leica Tissue Processor ASP  
676 300s) and embedding centre (Thermo histostar) performed with the SURF histology facility  
677 at The Queen's Medical Research Institute, University of Edinburgh. 10 µm sections were  
678 cut on a rotary microtome (Leica), adhered to poly-L-lysine coated slides, dewaxed by  
679 incubating in histoclear twice for ten minutes, rehydrated through an ethanol series and  
680 stained in 0.1% Toluidine Blue.

681

682 **Toluidine blue permeability analysis using Arabidopsis seedlings**

683

684 To assess cuticle integrity, toluidine blue staining assays were performed (61). For  
685 qualitative toluidine blue staining tests, etiolated seedlings were used. Seedlings were  
686 stratified in the dark, exposed to a 6h light flash and then grown for 4 days in darkness. They  
687 were then stained for 2 min in 0.05% w/v Toluidine blue solution with 0.1% v/v Tween 20  
688 and washed abundantly under tap water. Pictures were taken with a Keyence VHX900F  
689 digital microscope.

690

691 For quantitative toluidine blue staining test, 7-day old light-grown seedlings were  
692 stained in the same way. In order to extract toluidine blue and chlorophyll, the cotyledons  
693 of ten seedlings were collected and placed in 1mL of 80% ethanol for at least 3 hours in  
694 darkness. Toluidine blue content of the resulting solution was measured at 626nm with a  
695 spectrophotometer. This absorbance was then normalized using chlorophyll absorbance at  
696 430nm, a wavelength not absorbed by toluidine blue. 6 repetitions were performed per  
697 condition (Xing et al., 2013). Data were subjected to an ANOVA test, and where differences  
698 were detected, a Scheffe test was used to whether significant differences existed between  
699 specific genotypes.

700

701 **Seed shape analysis**

702

703 Percentages of misshapen seeds were counted from images taken with the VHX900F digital  
704 microscope (Keyence), using the cell counter extension of the ImageJ software. For each  
705 genotype, seeds from 4 distinct mother plants were analysed with approximately 1000

706 seeds analysed per mother plant. Data were subjected to an ANOVA test, and where  
707 differences were detected, a Scheffe test was used to whether significant differences  
708 existed between specific genotypes.

709

#### 710 **RNA extraction, cDNA synthesis, RNA seq**

711

712 Total RNA was extracted from 0.1 g of plant material, ground to fine powder in liquid  
713 nitrogen and resuspended by vortexing in 1ml Trizol (Ambion). After centrifugation at  
714 12,000 rpm in a microfuge for 10 minutes at 4°C, 0.2 vol chloroform were added to the  
715 supernatant, vortexed and spun again at 12,000 rpm for 15 minutes at 4°C. The upper,  
716 aqueous phase was collected and ethanol added to a final concentration of 35% ethanol and  
717 the mixture loaded on to a silica spun column (NEB biologicals NES-5-008) and spun at  
718 11,000 g for 30 seconds at room temperature. The bound RNA was washed with 700 µl  
719 wash buffer RW1 (Qiagen) and spun at 11,000 g for 30 sec, then washed twice with 500 µl  
720 wash buffer RPE (Qiagen) and spun at 11,000 g for 30 sec at RT each time, followed by a 2  
721 minute spin at 18,000g to dry the columns. The RNA was eluted from the columns with 40  
722 µl RNase-free water and its concentration was estimated by measuring the absorbance at  
723 260 nm using a 2 µl aliquot in a Nanodrop spectrophotometer.

724

725 For cDNA synthesis 1 µl anchored oligo-dT primer (1 µg/µl) and 1 µg total RNA were  
726 combined in a 10 µl volume and incubated at 65°C for 5 minutes to denature secondary  
727 structure then cooled rapidly on ice for 1 min. A 20 µl reverse transcriptase (RT) reaction  
728 was assembled with 1 µl 10 mM deoxyribonucleotide triphosphates (dNTP), 4 µl 5x RT  
729 Buffer (Promega), 3 µl water, 1 µl RNasin (Promega) and 1 µl MMLV RT (Promega M1701)  
730 and incubated at 42°C for 50 minutes then at 65°C for 15 minutes. The reactions were  
731 diluted ten-fold to 200 µl in 10 mM Tris-HCl (pH8.0) and 5 µl were used in PCR  
732 amplifications.

733

734 For RNAseq experiments, RNA samples were prepared as above and sent to  
735 Edinburgh Genomics, University of Edinburgh for quality control, cDNA preparation, library  
736 preparation and next generation sequencing (Illumina HiSeq). The quality of the raw reads  
737 was analysed using FastQC and sequences trimmed using Cutadapt implemented on the  
738 Galaxy server (<https://usegalaxy.org/>). Expression levels were quantified using Salmon (62)  
739 and the Marchantia transcriptome version 3.1 (<https://marchantia.info/>). Statistical analysis  
740 of the expression data used DESeq2 implemented in R studio. The raw data has been  
741 uploaded to the SRA database and is available after publication via the link  
742 <https://www.ncbi.nlm.nih.gov/sra/PRJNA999075>

743

#### 744 **Nuclei Quantification in Tak1, proEF1:MpZOU1 and Mpzou1-1**

745 The number of tdTomato nuclei in rhizoids were assessed in 6 weeks old thalli of PCD reporter  
746 lines (*proMp4g17600::Tdtomato*, *proMp8g07700::Tdtomato*, *proMp3g06430::Tdtomato*) in  
747 Tak1, *proEF1:MpZOU1* and *Mpzou1-1* grown on petri dishes and imaged using an AXIO Zoom  
748 V16 stereomicroscope (ZEISS, Oberkochen, Germany) equipped with a Plan-Neofluar 0.5x (NA  
749 0.19) objective and a mcherry-LP filter cube for Tdtomato imaging.

750

#### 751 **FDA-PI staining to distinguish living and dying rhizoids**

752 The FDA-PI live-death staining was performed on 19-day old thalli that had been  
753 grown on vertical agar plates covered by aluminum foil to shade the lower part of the  
754 plates, stimulating negative-phototropic growth of the rhizoids on the agar surface. The  
755 thalli were mounted on a microscope slide with the rhizoids covered by a cover glass in an  
756 FDA-PI solution (1  $\mu$ L FDA stock solution [2 mg in 1 ml acetone] dissolved in 1 ml  $\frac{1}{2}$  X MS  
757 with 10% sucrose, supplemented with 10  $\mu$ g/ml PI. FDA and PI were imaged simultaneously  
758 on the LSM710 (Zeiss), excitation 488 nm for FDA and 561nm for PI; emission was from 500-  
759 550 nm for FDA and from 600-700 nm for PI.  
760

## 761 **Figure legends**

762

### 763 **Figure 1 Phylogeny and features of ZOU proteins**

764 (A) Bayesian phylogeny, midpoint rooted, posterior probabilities are indicated for branches  
765 with >95% support. . The clades containing the MpZOU1 and MpZOU2 orthologues are  
766 highlighted with dark or light red branches, respectively. The ICE clade is highlighted with  
767 green branches. The numbering of bHLH proteins follows (19). Species abbreviations are At  
768 *Arabidopsis thaliana*, Mg *Mimulus guttifer*, Ac *Aquilegia coerulea*, Nc *Nymphae colorata*,  
769 Amtr *Amborella trichopoda*, Pa *Picea abies*, Sc *Salvinia cucullata*, Sm *Selaginella*  
770 *moellendorffii*, Ap *Anthoceros punctatus*, Pp *Physcomitrella patens*, Mp *Marchantia*  
771 *polymorpha*, Cb *Cylindrocystis brebissonii*, Cysp *Cylindrocystis* species. Different taxonomic  
772 groupings coloured as shown in box on left. All major land plant groups contain ZOU and ICE  
773 genes. (B) Schematic representation of the ZOU proteins with the conserved bHLH and ACTL  
774 domains indicated. The percentage amino acid identities between the bHLH and ACTL  
775 domains of the Marchantia and Arabidopsis proteins are indicated in blue and green,  
776 respectively. (C) Alignment of the bHLH domains (D) Alignment of the ACTL domains. The  
777 red triangles indicate the position at which the introns interrupt the protein coding  
778 sequences.  
779

779

### 780 **Figure 2. Conservation of ZOU and ICE protein properties**

781 (A) Schematic of full length and truncated ICE proteins (B) Controls for yeast two hybrid  
782 assays. Protein fusions to GAL4 DNA binding domains ("bait") and transcriptional activation  
783 domains ("prey") were tested against empty vector controls. Three serial X10 dilutions were  
784 plated and growth on minimal non selective (-LW) and selective (-LWHA) media is shown.  
785 Full length ICE proteins autoactivate and were not used for assays in (C) ZOU and ICE1  
786 proteins interact in yeast. (D) Dry seeds of wild-type (Col-0), mutants and complemented  
787 lines as indicated. Partially complemented seeds are indicated by an asterisk. Scale bar,  
788 200 $\mu$ m. (E) Quantification of misshapen dry seeds in different background. N=5,  
789 approximately 1000 seeds per repetition. \*\*\* indicates statistical differences with ANOVA  
790 and Sheffe tests (p-value 0.01). Error bars indicate standard deviation. (F) Toluidine blue  
791 assays on etiolated cotyledons of the same wild-type (Col-0), mutant and complemented  
792 lines. Scale bars 500 $\mu$ m. (G) Quantification of toluidine blue uptakes by the cotyledons of  
793 young seedlings, normalized to chlorophyll content. N= 6, 10 seedlings per repetition.. \*\*\*  
794 indicates statistical differences with ANOVA. Error bars indicate standard deviations.  
795

795

### 796 **Figure 3. Expression patterns of MpZOU1 and MpICE1 transcriptional reporters..**

797 Expression patterns of *GUS* reporter genes, Wild-type non-transgenic control is Tak1.  
798 (A to C) Whole mount of 20-days-old whole thallus. Scale bar, 500 $\mu$ m.

799 (D to F) Vibratome sectioned thallus. Scale bar, 100µm.  
800 (G to H) Vibratome section of gemma cups showing young gemmae, large round cells  
801 (arrows) are rhizoid precursors. Scale bar 100 µm.  
802 (I-J) Ventral surface of thallus at 3 days (I) and 19 days (J) after gemma sowing. Staining at  
803 the notch is indicated with red arrows, rhizoid primordia and rhizoids are also intensely  
804 stained. Scale bars 500 µm and 1mm.  
805 (K) Transverse longitudinal section through midrib of wax embedded 20 day old plants  
806 showing staining in ventral parenchyma and in scales. Scale bar 100 µm.  
807 (L – N) Ventral surface of thallus at day 6 (L), day 19 (M) and in transverse longitudinal  
808 section of 20 day old plant (N). Like *MpZOU1*, the *MpICE1* reporter is expressed at the  
809 notch, in rhizoid primordia and rhizoids, but it also shows weak expression in the dorsal air  
810 chambers (N). There is little expression in scales other than the youngest one. Scale bars  
811 500 µm, 1mm and 100 µm.  
812 (O – Q) Transverse longitudinal sections through wax embedded 20 day old plants. The  
813 approximate position of the sections shown in panels K,N,P and Q is shown schematically in  
814 (O). Both reporters are expressed around the notch, *MpZOU1* is ventral in expression  
815 whereas *MpICE1* is expressed dorsally and ventrally. Scale bars 100 µm. Ac air chamber, Sc  
816 Scale, dorsal surface uppermost in K, N, P – Q.

817

#### 818 **Figure 4. *MpZOU1* and *MpICE1* promote pegged rhizoid formation**

819 (A) Light micrographs (DIC) of rhizoids of 12 day old gemmalings of wild type (Tak2), loss of  
820 function mutants, a complemented *Mpzou1* mutant and *MpZOU1*-OE. In wild type, pegged  
821 rhizoids are indicated with red arrows, smooth rhizoids with white arrows. Smooth rhizoids  
822 typically have slightly wider bore than pegged. Scale bar 100 µM (B) Like wild-type (Tak1),  
823 rhizoids emerge from the ventral but not the dorsal epidermis of *MpZOU1*-OE. Scale bar  
824 1mm (C) Ventral surface of ten week old thallus of wild type and *MpZOU1*-OE (left panel). In  
825 wild type, bundles of pegged rhizoids are covered with red pigmented scales and grow  
826 parallel to thallus surface along the midrib (red arrow). Smooth rhizoids emerge outside the  
827 scales and grow away from the epidermis (white arrow), scale bar 1cm. DIC microscopy  
828 (middle panel, scale bar 100 µM) on the latter confirm that they are smooth rhizoids.  
829 Transverse sections through the midrib region (right panel, scale bar 100 µM) show pegged  
830 rhizoids under scales (Sc) at the midrib and larger, lighter staining smooth rhizoids (green  
831 arrows) towards the periphery. In *MpZOU1*-OE the rhizoids growing away from the thallus  
832 are all pegged (middle and right panels). (D) Light micrographs (DIC) of 12 day old  
833 gemmalings of *Mpice1* mutant and *MpICE1*-OE in wild type and *Mpice1* mutant  
834 backgrounds. *MpICE1* OE complements the *Mpice1* mutant phenotype, whereas *MpZOU1*  
835 OE does not. Scale bar 100 µM

836

#### 837 **Figure 5. *MpZOU1* controls pegged rhizoid programmed cell death**

838 (A) Expression of orthologues of dPCD-associated genes.  
839 (B-C) Expression pattern of *proMpDMP1* (B) and *proMpMCA-IIc* transcriptional reporters (C) in  
840 wild-type (Tak1) 2-week old thalli (left panels) and rhizoids (right panels). Bars 1mm (right  
841 panels) ; 100µm (left panels).  
842 (D-F) Expression pattern of *proMpDMP1* (left panel) and *proMpMCA-IIc* (right panel) in wild-  
843 type (Tak1) (D), *Mpzou1-1* (E) and *MpZOU1*-OE (F) in 6-week old thalli. Bar 2mm. White  
844 circles indicate visible nuclei, hashtag indicates the nucleus in the inset.



845 (G) Number of tdTomato nuclei observed in 6 weeks old thalli of PCD reporter lines in wild-  
846 type (Tak1), MpZOU1-OE and Mpzou1-1 genotypes. n=10, ordinary one-way ANOVA \*\*\*P-  
847 value<0.001 ; \*\*\*\* P-value<0.0001  
848 (H-J) Confocal tiling images of FDA-PI stained rhizoids of 19-day old thalli. Dead (PI-positive,  
849 FDA-negative) rhizoids are indicated by arrowheads in wild-type (Tak1) (H) and MpZOU1-OE  
850 (J), but are absent in Mpzou1-1 (I). Scale bar, 1mm.  
851 (K) Quantification of nuclear foci in wild-type (Tak1), Mpzou1-1, and MpZOU1-OE in  
852 substrate rhizoids at 19-day old thalli indicating more nuclei in Mpzou1-1, and less in  
853 MpZOU1-OE when compared to wild type. n=4, Mann Whitney test \*P-value<0.05.

854

### 855 **Figure 6. Terminal differentiation of pegged rhizoids ends with cell death**

856 (A) Confocal time-lapse imaging of a pegged rhizoid expressing *proMpZOU1:tdTomato-NLS*.  
857 Time indicated in minutes (min) corresponding to Video S2. The magenta arrowhead marks  
858 the first time frame after nuclear envelope breakdown, the white arrowheads marks the  
859 advancing front of peg formation reaching the tip of the rhizoid prior to cell death  
860 execution. (B) Confocal time-lapse imaging of a pegged and a smooth rhizoid expressing a  
861 double reporter (nuclear *proMpUBE2:mTurquoise-N7* [cyan], plasma membrane-bound  
862 *proMpUBE2:Scarlet1-Lti6b* [magenta]). Time indicated in minutes (min) corresponding to  
863 Video S1. The cyan arrowhead marks leakage of nuclear mTurquoise-N7 into the cytosol  
864 indicating nuclear envelope breakdown. Magenta arrowhead marks solubilization of  
865 Scarlet1-Lti6b into the cytosol, indicating endodomain shedding. White arrowhead marks  
866 even distribution of Scarlet1-Lti6b in the cell lumen, indicating vacuolar collapse. Yellow  
867 arrowhead marks leakage of Scarlet1-Lti6b into the extracellular space indicating plasma  
868 membrane disintegration. Scale bars are 50µm.

869

### 870 **Figure 7. MpZOU1 and MpICE1 promote water uptake**

871 (A) Confocal time lapse imaging of a pegged rhizoid expressing *proMpZOU1:tdTomato-NLS*  
872 (red signal). Red arrowhead marks nuclear envelope breakdown, followed by a diffusion of  
873 the non-membrane permeable fluorescein (green signal) into the lumen, indicating failure  
874 of plasma-membrane integrity (white arrowhead). Scale bars are 50µm.  
875 (B) Representative images of wild type (Tak1) and MpZOU1-OE thalli under well-watered  
876 conditions, regular photo on the right, Fv/Fm ratiometric image on the left.  
877 (C) Representative images of wild type (Tak1) and MpZOU1-OE thalli under well-watered  
878 conditions, regular photo on the right, Fv/Fm ratiometric image on the left. Images in B) and  
879 C) are 25 mm wide.  
880 (D) Quantification of Fv/Fm measurements in well-watered and drought-stressed thalli of  
881 Tak1 wild type and MpZOU1-OE. A Welch's two-sample t-tests indicates a non-significant  
882 (n.s.) PSII photochemical efficiency in well-watered conditions (p = 0.07225), but a highly  
883 significant difference in PSII photochemical efficiency in MpZOU1-OE under drought  
884 conditions (\*\*\*, p = 1.063e-15).  
885 (E) Gametophores of mutant lines are smaller than wild type and frequently desiccated  
886 (upper panel). The white lines indicate approximate position of the transverse sections of  
887 wax embedded stalks shown in the lower panels. Two bundles of internalized pegged  
888 rhizoids run up the stalks (arrows in middle row). In wild type all rhizoids are pegged, in the  
889 mutants there are fewer rhizoids and they are smooth, slightly wider in bore and lighter  
890 staining than pegged rhizoids as seen in high magnification images (bottom row). Scale bars  
891 are 500 µM in upper panel and 50 µM in lower panels.

892

## 893 **Supplementary Figures**

894

### 895 **Figure S1 The MpZOU1 and MpICE1 genes are expressed in rhizoids.**

896 (A-B) Confocal composite images of maximum Z-stack projections showing fluorescence of  
897 nuclear localized *pro*MpZOU1:NLS-TdTomato (A) and *pro*MpICE1:NLS-TdTomato (B)  
898 transcriptional reporter constructs. Expression can be seen in the underside of the thalli and  
899 in growing rhizoids (isolated nuclei, some indicated by arrowheads).

900 (C-D) Higher-resolution confocal images of *pro*MpZOU1:NLS-TdTomato (C) and *pro*MpICE1:NLS-  
901 TdTomato (D) overlaid with a transmitted light image showing expression in pegged rhizoids  
902 (PR) and a smooth rhizoid (SR), which could also be an immature pegged rhizoid. Scale bars  
903 are 1mm (A-B) or 0.2mm (C-D)

904

### 905 **Figure S2. Mpzou1 and Mpice1 mutant alleles produced by genome editing**

906 A. Schematic of MpZOU1 gene, filled rectangles indicate exons, untranslated regions are  
907 shown in blue and coding sequences in red. sgRNA1 and 2 target basic and loop regions of  
908 bHLH domain, respectively. B. Chromatograms showing sequence alteration in *Mpzou1-1*  
909 allele. C. Sequence of *Mpzou1* alleles. The sgRNA sequence is underlined in wild type (WT)  
910 and the PAM sequence shown in bold. *Mpzou1-1* and *Mpzou1-5* have the same lesion but  
911 were independent isolates. The alleles were generated with sgRNA1 except *Mpzou1-2* which  
912 was from sgRNA2. D. Schematic of MpICE1 gene, sgRNA targets basic region of bHLH domain.  
913 E. Sequence of *Mpice1* alleles. The insertion in *Mpice1-6* introduces premature stop codons.

914

### 915 **Figure S3. Rhizoid formation in Mpzou1 and Mpice1 mutants.**

916 (A) Light micrographs of Toluidine Blue stained transverse sections of wax embedded midrib  
917 region of thallus of wild type and mutants. The right hand panels are higher magnification  
918 images of the sections in left hand panels. In wild type (Tak2) the smooth rhizoids are at the  
919 periphery of the sections and are slightly larger in bore and lighter staining than the pegged  
920 rhizoids, which are mainly in bundles under the scales (Sc) at the midrib. In the mutants,  
921 smooth rhizoids (note lighter staining and wider bore) replace pegged rhizoids in midrib  
922 region. Yellow arrows indicate rhizoids with partial peg formation in mutants. (B) Light  
923 micrographs of Toluidine Blue stained transverse sections of resin embedded  
924 antheriodophore stalks of wild type and *Mpzou1-6* mutant. White arrow indicates a pegged  
925 rhizoid in one of the two grooves of pegged rhizoids that run up the stalks. In the mutant,  
926 several rhizoids have pegs (yellow arrow) but they are much shorter than in wild type. Red  
927 arrows smooth rhizoids, white arrows pegged rhizoids, yellow arrows rhizoids with partially  
928 developed pegs. Scale bars 100 μM

929

### 930 **Figure S4. Effect of MpNAC5 on pegged rhizoid development**

931 (A) Schematic of MpNAC5 (*Mp6g20920*) gene structure. Exons shown as boxes, introns as  
932 lines, coding sequences are coloured. Red arrow indicates position of sgRNA used for  
933 editing. (B). Sequence chromatograms and alignments for two mutant alleles obtained. Bold  
934 indicates PAM sequence, sgRNA sequence is underlined, indels are in red, substitutions in  
935 blue. Both alleles introduce frameshifts and premature termination of translation and are  
936 likely nulls. (C). Light micrographs of rhizoids from 7 day old mutant plants, pegged rhizoids  
937 indicated with red arrows. Scale bars 100μM

938

939 **Figure S5. Effects of *Mpzou1-1* and *MpZOU1*-OE on numbers of living rhizoids in thalli**  
940 (A-C) Confocal tile scans of Tak1, *Mpzou1-1*, and *MpZOU1*-OE rhizoids expressing nuclear  
941 localized mTurquoise and plasma-membrane localized mScarlet-I (*proMpUBE2:mTurquoise-*  
942 *N7*, *proMpUBE2:ScarletI-Lti6b*). Imaging of 19-day old thalli in that have been cultivated in  
943 microscopic chambers on agar. The substrate rhizoids grow through the agar and along the  
944 chamber bottom allowing convenient imaging from below. A) Wild-type (Tak1). B) *Mpzou1-*  
945 *1*. C) *MpZOU1*-OE. Inset shows a single tile at higher magnification, dashed squares indicate  
946 the location of the tile that is shown in the insets. Scale bars are 1mm, 100µm in the insets.  
947

948 **Table S1. *MpZOU1* and *MpICE1* control pegged rhizoid formation**

949 (A) Mean number of pegged rhizoids,  $\pm$  standard error of mean (n=9-10), in 12 day old  
950 gemmalings.  
951 (B) Mean diameter of rhizoids,  $\pm$  standard error of mean (n>23) in 12 day old gemmalings,  
952 measured from DIC micrographs of whole mount fresh tissue. For wild type (Tak2), rhizoids  
953 with pegs were measured separately from those lacking pegs (i.e. mainly smooth with a few  
954 pegged pre-differentiation). Statistical analysis (ANOVA followed by Dunn's post hoc test  
955 Bonferoni corrected) indicated significant differences ( $p<0.01$ ) between groups a and b but  
956 not within the two groups.  
957

958 **Table S2 Cell wall, cell death and redox genes are down-regulated in *Mpzou1* and *Mpice1***  
959 **mutants.** Selected genes down-regulated in both *Mpzou1* and *Mpice1* mutants are shown  
960 together with the log2 fold change values.  
961

962 **Supplementary Data**

964 **Data S1 Phylogenetic analysis of VND, Metacaspases, Aspartic proteases and DMP-Like**  
965 **proteins.**

966 (A-D) Four Bayesian phylogenies are provided and legends included on the figures.  
967

968 **Data S2 RNAseq analysis of genes down-regulated in *Mpzou1* and *Mpice1* mutants lacking**  
969 **pegged rhizoids**

970 Excel data sheet with four sheets, the first sheet is a README with legends to explain the  
971 succeeding three sheets. Analysis was on total tissue of 12 day old gemmalings and four  
972 biological replicates were used.  
973

974 **Data S3. Primers used**

975 Excel data sheet with details of oligonucleotide primers used.  
976

977 **Video S1. Cellular decompartmentalization in dying pegged rhizoids**

978 Confocal time-lapse imaging of a pegged and a smooth rhizoid expressing a double reporter  
979 (nuclear *proMpUBE2:mTurquoise-N7* [cyan], plasma membrane-bound *proMpUBE2:ScarletI-*  
980 *Lti6b* [magenta]). Time indicated in minutes (min). Note how the smooth rhizoid continues  
981 growing while the pegged rhizoid has arrested tip growth prior to cell death execution.  
982 Corresponding to Figure 5B, scale bar is 50µm.  
983

984 **Video S2. Peg formation precedes acropetally in rhizoids and precedes cell death**

985 Confocal time-lapse imaging of a pegged rhizoid expressing *proMpZOU1:tdTomato-NLS*  
986 (*magenta*), *time* indicated in minutes (min). Corresponding to Figure 5A, scale bar is 50µm.  
987

### 988 **Video S3. Entry of fluorescein upon cell death**

989 Confocal time lapse imaging of a pegged rhizoid expressing *proMpZOU1:tdTomato-NLS* (red  
990 signal) and stained with non-membrane permeable fluorescein (green signal). Note how the  
991 fluorescein enters the lumen of the pegged rhizoid after cell death execution visualized by  
992 nuclear envelope breakdown (disappearance of the red nuclear signal). Corresponding to  
993 Figure 5C, scale bar is 50µm.  
994  
995  
996

### 997 References

- 998 1. M. Zinkgraf, S. Gerttula, A. Groover, Transcript profiling of a novel plant meristem,  
999 the monocot cambium. *J Integr Plant Biol* **59**, 436-449 (2017).
- 1000 2. M. N. Puttick *et al.*, The Interrelationships of Land Plants and the Nature of the  
1001 Ancestral Embryophyte. *Curr Biol* **28**, 733-745 e732 (2018).
- 1002 3. S. Woudenberg, J. Renema, A. M. F. Tomescu, B. De Rybel, D. Weijers, Deep origin  
1003 and gradual evolution of transporting tissues: Perspectives from across the land  
1004 plants. *Plant Physiol* **190**, 85-99 (2022).
- 1005 4. N. Akiyoshi *et al.*, Involvement of VNS NAC-domain transcription factors in tracheid  
1006 formation in *Pinus taeda*. *Tree Physiol* **40**, 704-716 (2020).
- 1007 5. M. Kubo *et al.*, Transcription switches for protoxylem and metaxylem vessel  
1008 formation. *Genes Dev* **19**, 1855-1860 (2005).
- 1009 6. M. Ohtani, N. Akiyoshi, Y. Takenaka, R. Sano, T. Demura, Evolution of plant  
1010 conducting cells: perspectives from key regulators of vascular cell differentiation. *J*  
1011 *Exp Bot* **68**, 17-26 (2017).
- 1012 7. R. Ligrone, J. G. Duckett, K. S. Renzaglia, Conducting tissues and phyletic  
1013 relationships of bryophytes. *Philos T Roy Soc B* **355**, 795-813 (2000).
- 1014 8. D. C. Scheirer, Differentiation of Bryophyte Conducting Tissues - Structure and  
1015 Histochemistry. *B Torrey Bot Club* **107**, 298-307 (1980).
- 1016 9. R. Ligrone, K. C. Vaughn, K. S. Renzaglia, J. P. Knox, J. G. Duckett, Diversity in the  
1017 distribution of polysaccharide and glycoprotein epitopes in the cell walls of  
1018 bryophytes: new evidence for the multiple evolution of water-conducting cells. *New*  
1019 *Phytol* **156**, 491-508 (2002).
- 1020 10. B. Xu *et al.*, Contribution of NAC transcription factors to plant adaptation to land.  
1021 *Science* **343**, 1505-1508 (2014).
- 1022 11. E. J. Bowen, A note on the conduction of water in *Fimbriaria bleumeana*. *Ann Bot-*  
1023 *London* **49**, 844-848 (1935).
- 1024 12. J. G. Duckett, R. Ligrone, K. S. Benzaglia, S. Pressel, Pegged and smooth rhizoids in  
1025 complex thalloid liverworts (Marchantiopsida): structure, function and evolution.  
1026 *Botanical Journal of the Linnean Society* **174**, 68-92 (2014).
- 1027 13. K. Goebel, Organography of Plants, Part II. *English translation by I.B. Balfour. Oxford.*,  
1028 46-47 (1905).
- 1029 14. M. McConaha, Ventral structures effecting capillarity in the Marchantiales. *Am J Bot*  
1030 **28**, 301-306 (1941).

- 1031 15. G. Denay *et al.*, Endosperm breakdown in Arabidopsis requires heterodimers of the  
1032 basic helix-loop-helix proteins ZHOUP1 and INDUCER OF CBP EXPRESSION 1.  
1033 *Development* **141**, 1222-1227 (2014).
- 1034 16. C. Fourquin *et al.*, Mechanical stress mediated by both endosperm softening and  
1035 embryo growth underlies endosperm elimination in Arabidopsis seeds. *Development*  
1036 **143**, 3300-3305 (2016).
- 1037 17. S. Yang *et al.*, The endosperm-specific ZHOUP1 gene of Arabidopsis thaliana regulates  
1038 endosperm breakdown and embryonic epidermal development. *Development* **135**,  
1039 3501-3509 (2008).
- 1040 18. N. M. Doll *et al.*, Endosperm cell death promoted by NAC transcription factors  
1041 facilitates embryo invasion in Arabidopsis. *Current Biology*.
- 1042 19. B. Catarino, A. J. Hetherington, D. M. Emms, S. Kelly, L. Dolan, The Stepwise Increase  
1043 in the Number of Transcription Factor Families in the Precambrian Predated the  
1044 Diversification of Plants On Land. *Mol Biol Evol* **33**, 2815-2819 (2016).
- 1045 20. B. J. Harris, C. J. Harrison, A. M. Hetherington, T. A. Williams, Phylogenomic Evidence  
1046 for the Monophyly of Bryophytes and the Reductive Evolution of Stomata. *Curr Biol*  
1047 **30**, 2001-2012 e2002 (2020).
- 1048 21. Q. Kong *et al.*, Regulatory switch enforced by basic helix-loop-helix and ACT-domain  
1049 mediated dimerizations of the maize transcription factor R. *Proc Natl Acad Sci U S A*  
1050 **109**, E2091-2097 (2012).
- 1051 22. H. Seo *et al.*, Intragenic suppressors unravel the role of the SCREAM ACT-like domain  
1052 for bHLH partner selectivity in stomatal development. *Proc Natl Acad Sci U S A* **119**,  
1053 (2022).
- 1054 23. K. C. Moriya *et al.*, Stomatal regulators are co-opted for seta development in the  
1055 astomatous liverwort Marchantia polymorpha. *Nat Plants* **9**, 302-314 (2023).
- 1056 24. T. E. Kongsted, B. J. Glover, Phylogenetic analysis of bHLH classes III and IV in land  
1057 plants and their algal relatives. *New Phytol* **240**, 1717-1721 (2023).
- 1058 25. A. Thamm, T. E. Saunders, L. Dolan, MpFEW RHIZOIDS1 miRNA-Mediated Lateral  
1059 Inhibition Controls Rhizoid Cell Patterning in Marchantia polymorpha. *Curr Biol* **30**,  
1060 1905-1915 e1904 (2020).
- 1061 26. M. Shimamura, Marchantia polymorpha: Taxonomy, Phylogeny and Morphology of a  
1062 Model System. *Plant Cell Physiol* **57**, 230-256 (2016).
- 1063 27. A. Putarjunan *et al.*, Bipartite anchoring of SCREAM enforces stomatal initiation by  
1064 coupling MAP kinases to SPEECHLESS. *Nat Plants* **5**, 742-754 (2019).
- 1065 28. H. Proust *et al.*, RSL Class I Genes Controlled the Development of Epidermal  
1066 Structures in the Common Ancestor of Land Plants. *Curr Biol* **26**, 93-99 (2016).
- 1067 29. F. Feng *et al.*, OPAQUE11 Is a Central Hub of the Regulatory Network for Maize  
1068 Endosperm Development and Nutrient Metabolism. *Plant Cell* **30**, 375-396 (2018).
- 1069 30. B. Bollhoner *et al.*, The function of two type II metacaspases in woody tissues of  
1070 Populus trees. *New Phytol* **217**, 1551-1565 (2018).
- 1071 31. B. Bollhoner *et al.*, Post mortem function of AtMC9 in xylem vessel elements. *New*  
1072 *Phytol* **200**, 498-510 (2013).
- 1073 32. Y. Olvera-Carrillo *et al.*, A Conserved Core of Programmed Cell Death Indicator Genes  
1074 Discriminates Developmentally and Environmentally Induced Programmed Cell  
1075 Death in Plants. *Plant Physiol* **169**, 2684-2699 (2015).
- 1076 33. Y. S. van Ekelburg *et al.*, Spatial and temporal regulation of parent-of-origin allelic  
1077 expression in the endosperm. *Plant Physiol* **191**, 986-1001 (2023).

- 1078 34. N. Niu *et al.*, EAT1 promotes tapetal cell death by regulating aspartic proteases  
1079 during male reproductive development in rice. *Nat Commun* **4**, 1445 (2013).
- 1080 35. Y. Lee, M. C. Rubio, J. Alassimone, N. Geldner, A mechanism for localized lignin  
1081 deposition in the endodermis. *Cell* **153**, 402-412 (2013).
- 1082 36. J. L. Bowman *et al.*, Insights into Land Plant Evolution Garnered from the *Marchantia*  
1083 *polymorpha* Genome. *Cell* **171**, 287-304 e215 (2017).
- 1084 37. M. D. Jackson, H. Xu, S. Duran-Nebreda, P. Stamm, G. W. Bassel, Topological analysis  
1085 of multicellular complexity in the plant hypocotyl. *Elife* **6**, (2017).
- 1086 38. H. He *et al.*, The Arabidopsis mediator complex subunit 8 regulates oxidative stress  
1087 responses. *Plant Cell* **33**, 2032-2057 (2021).
- 1088 39. A. J. Villarreal, B. J. Crandall-Stotler, M. L. Hart, D. G. Long, L. L. Forrest, Divergence  
1089 times and the evolution of morphological complexity in an early land plant lineage  
1090 (*Marchantiopsida*) with a slow molecular rate. *New Phytol* **209**, 1734-1746 (2016).
- 1091 40. B. J. Harris *et al.*, Divergent evolutionary trajectories of bryophytes and  
1092 tracheophytes from a complex common ancestor of land plants. *Nat Ecol Evol* **6**,  
1093 1634-1643 (2022).
- 1094 41. J. Wang *et al.*, SMB controls decompartmentalization in Arabidopsis root cap cells to  
1095 execute programmed cell death. *bioRxiv*, 2023.2008.2010.552584 (2023).
- 1096 42. A. Grimault *et al.*, ZmZHOUP1, an endosperm-specific basic helix-loop-helix  
1097 transcription factor involved in maize seed development. *Plant J* **84**, 574-586 (2015).
- 1098 43. E. Strasburger, Einige Bemerkungen zur Frage nach der "doppelten  
1099 Befruchtung" bei den Angiospermen. *Botanische Zeitung* **58**, 294-315 (1900).
- 1100 44. A. M. Florez-Rueda, C. M. Miguel, D. D. Figueiredo, Comparative transcriptomics of  
1101 seed nourishing tissues: uncovering conserved and divergent pathways in seed  
1102 plants. *BioRxiv*, (2023).
- 1103 45. S. Honkanen *et al.*, The Mechanism Forming the Cell Surface of Tip-Growing Rooting  
1104 Cells Is Conserved among Land Plants. *Curr Biol* **26**, 3238-3244 (2016).
- 1105 46. M. Takenaka *et al.*, Direct transformation and plant regeneration of the haploid  
1106 liverwort *Marchantia polymorpha* L. *Transgenic Res* **9**, 179-185 (2000).
- 1107 47. M. M. Kanaoka *et al.*, SCREAM/ICE1 and SCREAM2 specify three cell-state  
1108 transitional steps leading to arabidopsis stomatal differentiation. *Plant Cell* **20**, 1775-  
1109 1785 (2008).
- 1110 48. S. F. Altschul, W. Gish, W. Miller, E. W. Myers, D. J. Lipman, Basic local alignment  
1111 search tool. *J Mol Biol* **215**, 403-410 (1990).
- 1112 49. P. Kerchev *et al.*, Activation of auxin signalling counteracts photorespiratory H<sub>2</sub>O<sub>2</sub>-  
1113 dependent cell death. *Plant Cell Environ* **38**, 253-265 (2015).
- 1114 50. N. R. Baker, Chlorophyll fluorescence: a probe of photosynthesis in vivo. *Annu Rev*  
1115 *Plant Biol* **59**, 89-113 (2008).
- 1116 51. Q. Lu *et al.*, Arabidopsis homolog of the yeast TREX-2 mRNA export complex:  
1117 components and anchoring nucleoporin. *Plant J* **61**, 259-270 (2010).
- 1118 52. M. Karimi, A. Bleys, R. Vanderhaeghen, P. Hilson, Building blocks for plant gene  
1119 assembly. *Plant Physiol* **145**, 1183-1191 (2007).
- 1120 53. K. Ishizaki *et al.*, Development of Gateway Binary Vector Series with Four Different  
1121 Selection Markers for the Liverwort *Marchantia polymorpha*. *PLoS One* **10**, e0138876  
1122 (2015).

- 1123 54. R. A. Jefferson, T. A. Kavanagh, M. W. Bevan, GUS fusions: beta-glucuronidase as a  
1124 sensitive and versatile gene fusion marker in higher plants. *EMBO J* **6**, 3901-3907  
1125 (1987).
- 1126 55. J. Schindelin *et al.*, Fiji: an open-source platform for biological-image analysis. *Nat*  
1127 *Methods* **9**, 676-682 (2012).
- 1128 56. S. S. Sugano *et al.*, Efficient CRISPR/Cas9-based genome editing and its application to  
1129 conditional genetic analysis in *Marchantia polymorpha*. *PLoS One* **13**, e0205117  
1130 (2018).
- 1131 57. Y. Naito, K. Hino, H. Bono, K. Ui-Tei, CRISPRdirect: software for designing CRISPR/Cas  
1132 guide RNA with reduced off-target sites. *Bioinformatics* **31**, 1120-1123 (2015).
- 1133 58. K. Ishizaki, S. Chiyoda, K. T. Yamato, T. Kohchi, *Agrobacterium*-mediated  
1134 transformation of the haploid liverwort *Marchantia polymorpha* L., an emerging  
1135 model for plant biology. *Plant Cell Physiol* **49**, 1084-1091 (2008).
- 1136 59. A. Kubota, K. Ishizaki, M. Hosaka, T. Kohchi, Efficient *Agrobacterium*-mediated  
1137 transformation of the liverwort *Marchantia polymorpha* using regenerating thalli.  
1138 *Biosci Biotechnol Biochem* **77**, 167-172 (2013).
- 1139 60. S. J. Clough, A. F. Bent, Floral dip: a simplified method for *Agrobacterium*-mediated  
1140 transformation of *Arabidopsis thaliana*. *Plant J* **16**, 735-743 (1998).
- 1141 61. T. Tanaka, H. Tanaka, C. Machida, M. Watanabe, Y. Machida, A new method for rapid  
1142 visualization of defects in leaf cuticle reveals five intrinsic patterns of surface defects  
1143 in *Arabidopsis*. *Plant J* **37**, 139-146 (2004).
- 1144 62. R. Patro, G. Duggal, M. I. Love, R. A. Irizarry, C. Kingsford, Salmon provides fast and  
1145 bias-aware quantification of transcript expression. *Nat Methods* **14**, 417-419 (2017).
- 1146

1147

## 1148 **Acknowledgements**

1149 The authors thank Kenta Moriya and Jeff Duckett for helpful comments on the manuscript  
1150 and discussion. JG thanks Victor Jones for patient instruction on how to work with  
1151 *Marchantia*, Catherine Kidner, Andrew Hudson and Al Ivens for bioinformatics advice.  
1152 Sequencing was carried out by Edinburgh Genomics, The University of Edinburgh, which is  
1153 partly supported with core funding from the Natural Environment Research Council (UKSBS  
1154 PR18037). Y-TL, JLM and PG were supported by Darwin Trust of Edinburgh, JLM was also  
1155 supported by INRAE, France. AH, SG--S, HM, FS, AC and SF were exchange visitors supported  
1156 by the EU ERASMUS scheme. MKN acknowledges funding from the European Research  
1157 Council (ERC) (StG PROCELLDEATH 639234 and CoG EXECUT.ER 864952) as well as  
1158 the Research Foundation – Flanders (FWO) project No. G041118N. JG is grateful to the  
1159 Gatsby Charitable Trust for a 15k grant to exceptional researchers to support PG lab expenses  
1160 .

1161

1162 **Author Contributions**

1163 Y-TL, JLM, NB and FDW performed the majority of the experiments with help and supervision  
1164 from GI, NDF, MKN and JG. PG, AH, SG--S, HM, FS, AC, SF and EdL contributed experimental  
1165 resources and support. TK and RN helped initiate the project and contributed training and  
1166 intellectual input. PC contributed transgenic lines with supervision and support from SS. Y-  
1167 TL, JLM, GI, MKN and JG wrote the paper with input from all authors. All authors checked and  
1168 approved the manuscript.

1169

1170 **Competing interests**

1171 The authors declare no competing interests

1172

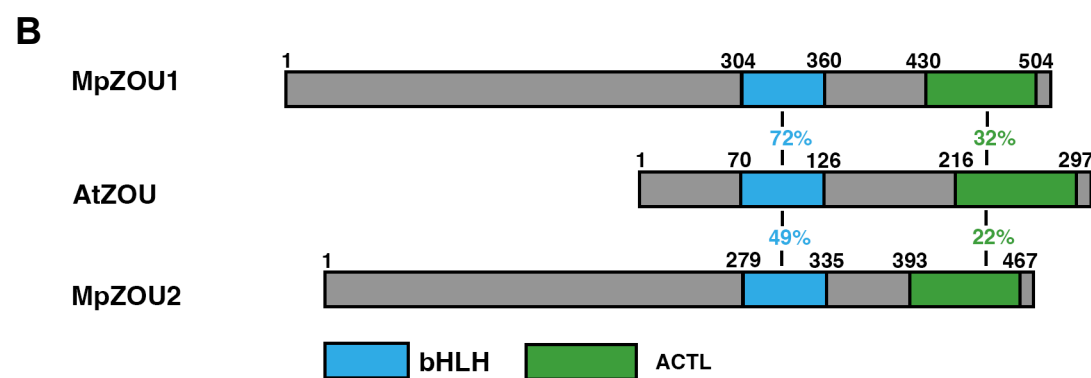
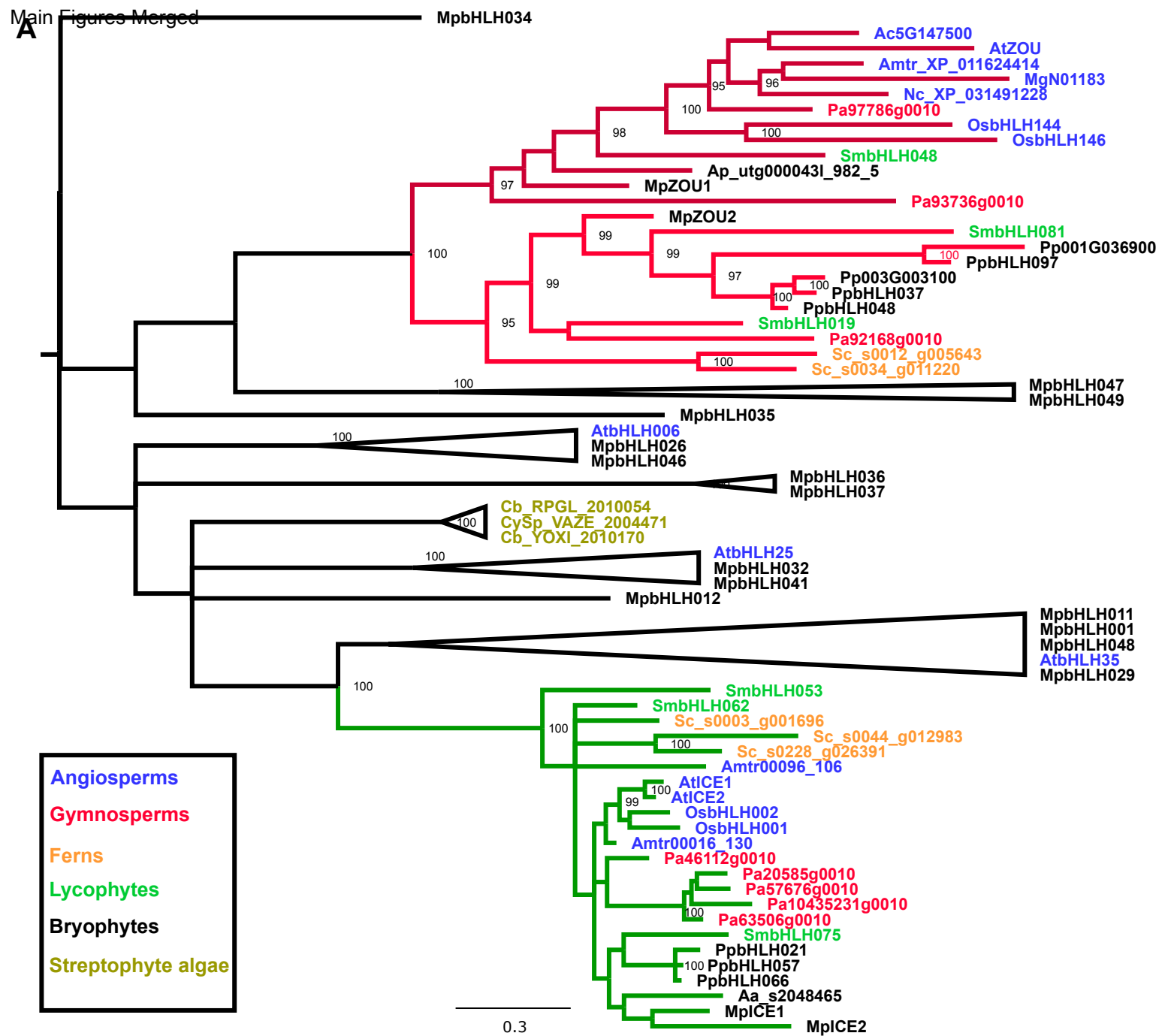
1173 **Materials and Correspondence**

1174 All data is available in the main text or the supplemental figures/tables. The raw data for the  
1175 RNAseq experiment has been deposited in the NCBI SRA databases under the BioProject  
1176 accession PRJNA999075. Request for materials should be addressed to JG.

1177

1178





**C**

Sequence alignment of bHLH domain (residues 1-504) for AtZOU, MpZOU1, and MpZOU2. A red triangle points to a conserved residue at position 430.

```

AtZOU  DHEIHIWTERERRKKMRDMFSK L HALLPQLIPKADKSTIVDEAVSS IKSLEQLTQKLL
MpZOU1 DHEIHIWTERERRKKMNGMFSTLHSLPLHNSKADKSTIVDEATINYIQTLGTMKGL
MpZOU2 QR ESHIWSERQRRKGMNH L FSTLRSLLPQPTSK TDKSTVVSEI I I KYIQGLQVK L DDEL
  
```

**D**

Sequence alignment of ACTL domain (residues 1-504) for AtZOU, MpZOU1, and MpZOU2. A red triangle points to a conserved residue at position 467.

```

AtZOU  RNVVLTICGNEAF F NLCV PKHK P GVFITSV CYLFEKYNMEVLFANVSSNVFWSTYVIQAQV
MpZOU1 KNVVLTNMCGNDAF ITICSPRGR LGLLCRVLFVIESHNLHVLNAHICTTNDTIMYMVHAQT
MpZOU2 PNVALHTISGNNAFITMS S PKKR -GLFCRILLIMQSHK L AVLNAHISTSNATVFFCLHVM T
  
```

Conserved residues in ACTL domain:

```

AtZOU  N - P S C E N Q L L G N G L G - V V D V F K Q V
MpZOU1 T - - - - E D Q - - - - L G N S D M L N I A L
MpZOU2 P E P G C D F P - - - - - K E A L Q T A L
  
```

### Figure 1 Phylogeny and features of ZOU proteins

(A) Bayesian phylogeny, midpoint rooted, posterior probabilities are indicated for branches with >95% support. . The clades containing the MpZOU1 and MpZOU2 orthologues are highlighted with dark or light red branches, respectively. The ICE clade is highlighted with green branches. The numbering of bHLH proteins follows (19). Species abbreviations are At *Arabidopsis thaliana*, Mg *Mimulus guttifer*, Ac *Aquilegia coerulea*, Nc *Nymphae colorata*, Amtr *Amborella trichopada*, Pa *Picea abies*, Sc *Salvinia cucullata*, Sm *Selaginella moellendorffii*, Ap *Anthoceros punctatus*, Pp *Physcomitrella patens*, Mp *Marchantia polymorpha*, Cb *Cylindrocystis brebissonii*, Cysp *Cylindrocystis* species. Different taxonomic groupings coloured as shown in box on left. All major land plant groups contain ZOU and ICE genes. (B) Schematic representation of the ZOU proteins with the conserved bHLH and ACTL domains indicated. The percentage amino acid identities between the bHLH and ACTL domains of the Marchantia and Arabidopsis proteins are indicated in blue and green, respectively. (C) Alignment of the bHLH domains (D) Alignment of the ACTL domains. The red triangles indicate the position at which the introns interrupt the protein coding sequences.

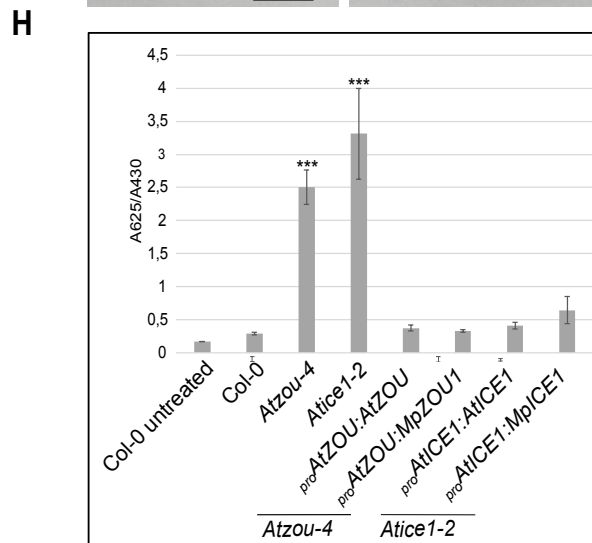
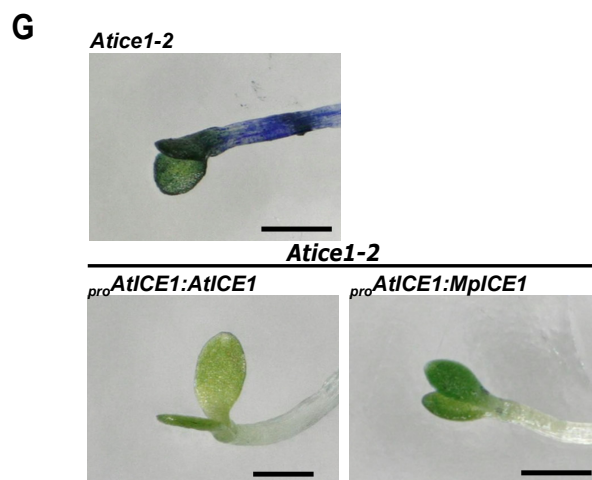
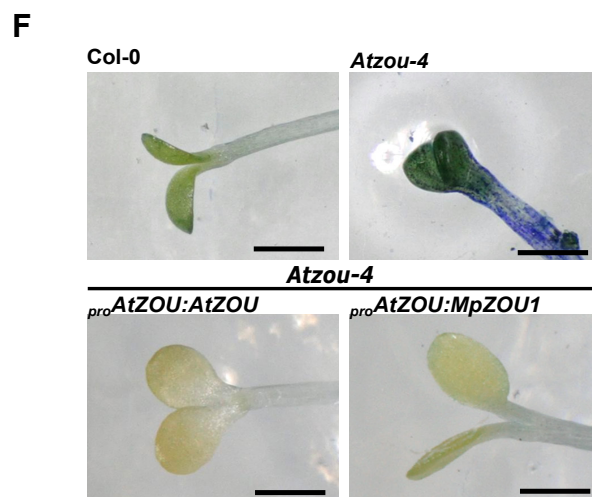
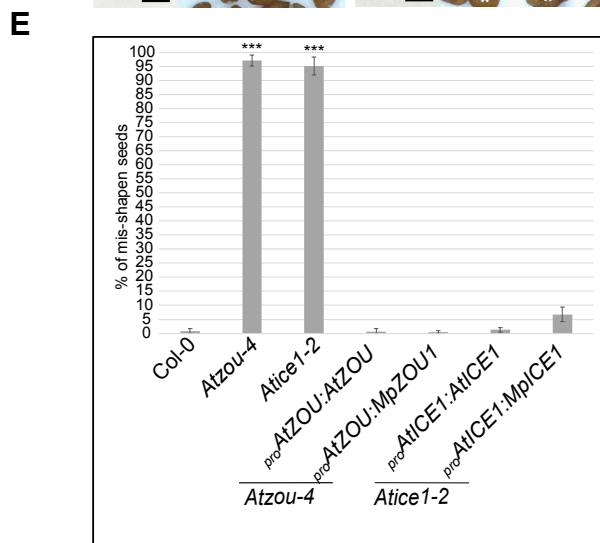
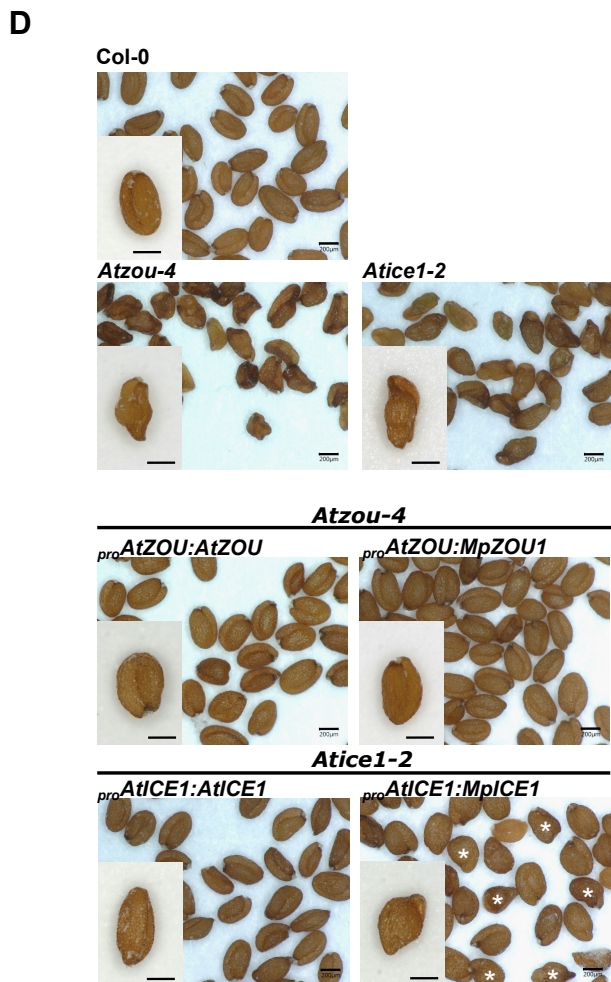
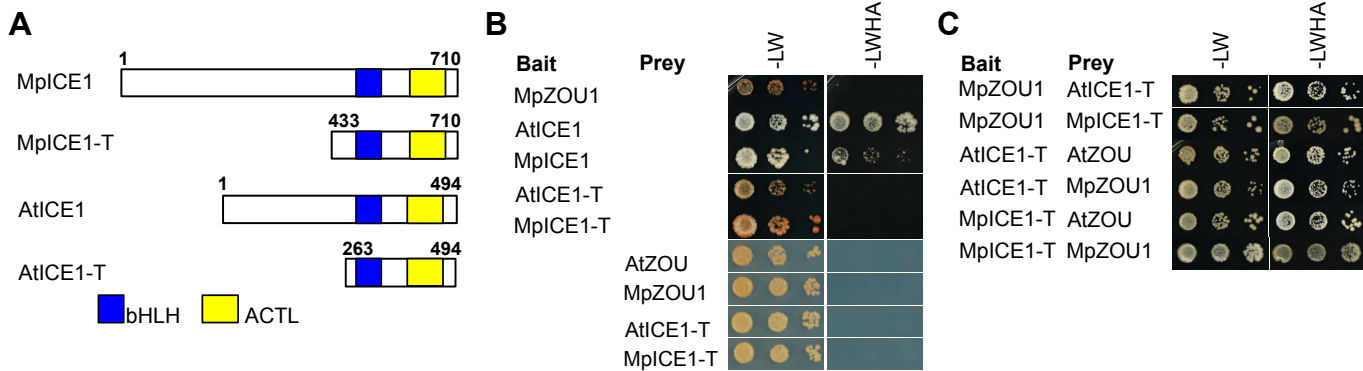


## Figure 2. Conservation of ZOU and ICE protein properties

(A) Schematic of full length and truncated ICE proteins (B) Controls for yeast two hybrid assays. Protein fusions to GAL4 DNA binding domains ("bait") and transcriptional activation domains ("prey") were tested against empty vector controls. Three serial X10 dilutions were plated and growth on minimal non selective (-LW) and selective (-LWHA) media is shown. Full length ICE proteins autoactivate and were not used for assays in (C) ZOU and ICE1 proteins interact in yeast. (D) Dry seeds of wild-type (Col-0), mutants and complemented lines as indicated. Partially complemented seeds are indicated by an asterisk. Scale bar, 200 $\mu$ m. (E) Quantification of misshapen dry seeds in different background. N=5, approximately 1000 seeds per repetition. \*\*\* indicates statistical differences with ANOVA and Sheffe tests (p-value 0.01). Error bars indicate standard deviation. (F) Toluidine blue assays on etiolated cotyledons of the same wild-type (Col-0), mutant and complemented lines. Scale bars 500 $\mu$ m. (G) Quantification of toluidine blue uptakes by the cotyledons of young seedlings, normalized to chlorophyll content. N= 6, 10 seedlings per repetition.. \*\*\* indicates statistical differences with ANOVA. Error bars indicate standard deviations.

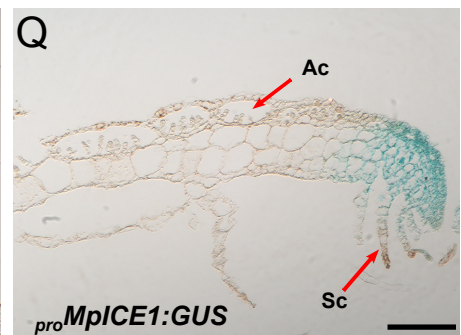
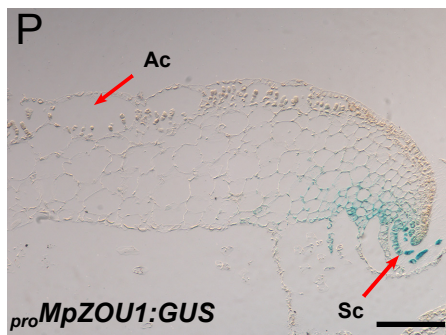
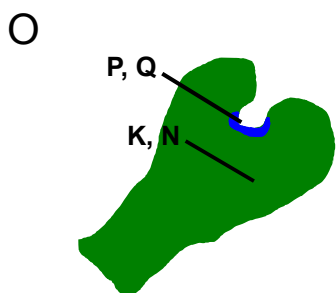
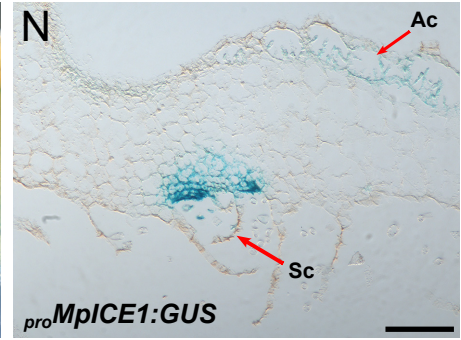
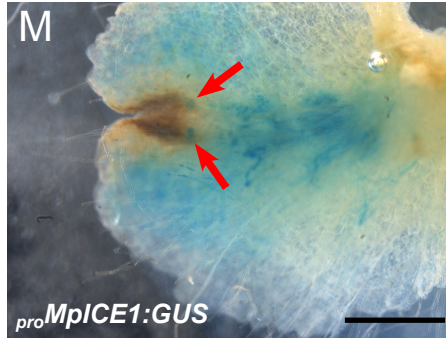
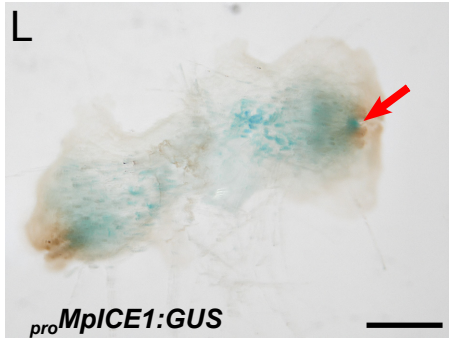
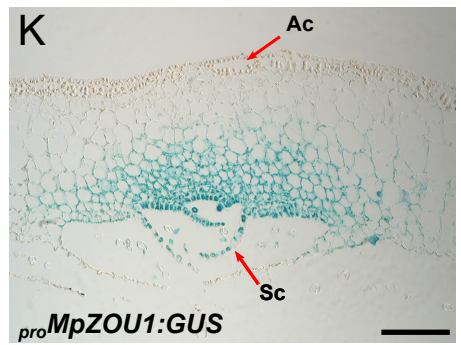
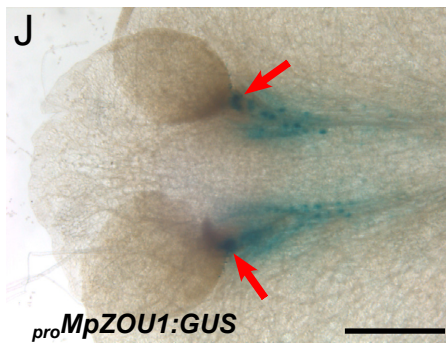
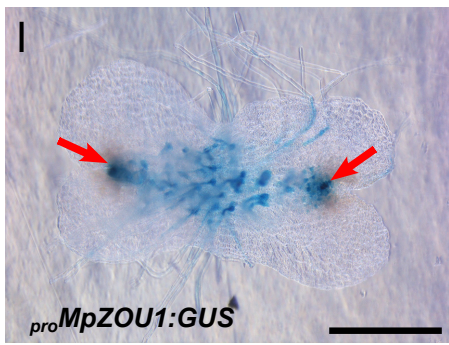
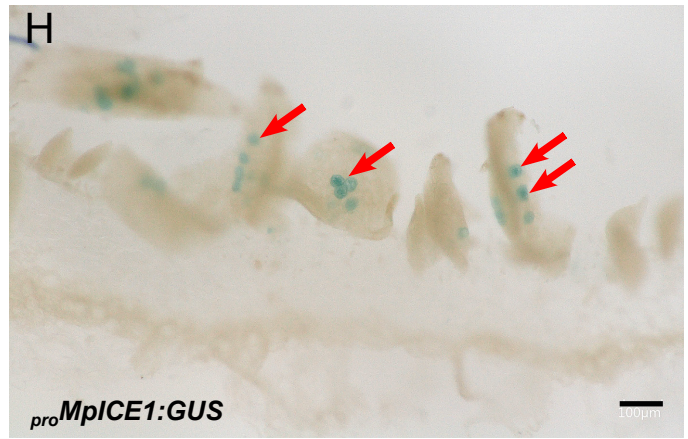
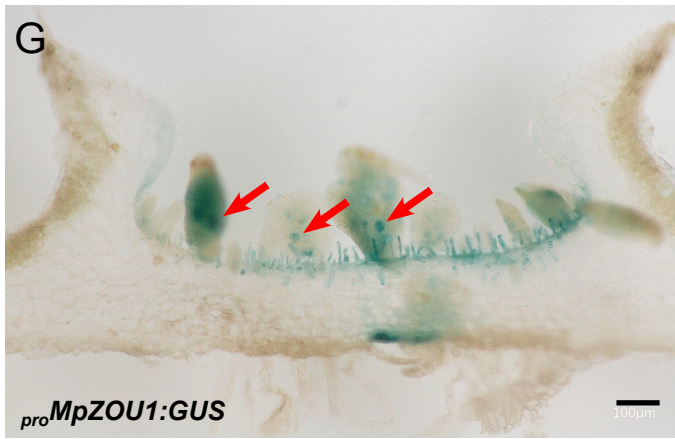
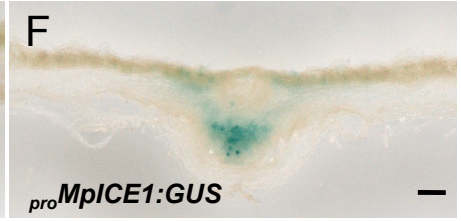
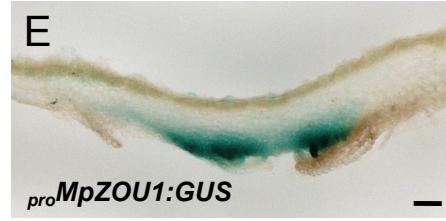
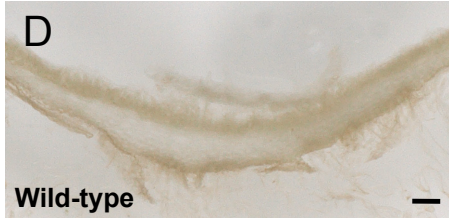
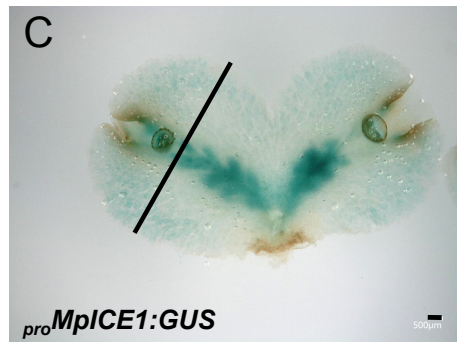


**Figure 3. Expression patterns of MpZOU1 and MpICE1 transcriptional reporters..**

Expression patterns of *GUS* reporter genes, Wild-type non-transgenic control is Tak1.

(A to C) Whole mount of 20-days-old whole thallus. Scale bar, 500µm.

(D to F) Vibratome sectioned thallus. Scale bar, 100µm.

(G to H) Vibratome section of gemma cups showing young gemmae, large round cells (arrows) are rhizoid precursors. Scale bar 100 µm.

(I-J) Ventral surface of thallus at 3 days (I) and 19 days (J) after gemma sowing. Staining at the notch is indicated with red arrows, rhizoid primordia and rhizoids are also intensely stained. Scale bars 500 µm and 1mm.

(K) Transverse longitudinal section through midrib of wax embedded 20 day old plants showing staining in ventral parenchyma and in scales. Scale bar 100 µm.

(L – N) Ventral surface of thallus at day 6 (L), day 19 (M) and in transverse longitudinal section of 20 day old plant (N). Like MpZOU1, the MpICE1 reporter is expressed at the notch, in rhizoid primordia and rhizoids, but it also shows weak expression in the dorsal air chambers (N). There is little expression in scales other than the youngest one. Scale bars 500 µm, 1mm and 100 µm.

(O – Q) Transverse longitudinal sections through wax embedded 20 day old plants. The approximate position of the sections shown in panels K,N,P and Q is shown schematically in (O). Both reporters are expressed around the notch, MpZOU1 is ventral in expression whereas MpICE1 is expressed dorsally and ventrally. Scale bars 100 µm. Ac air chamber, Sc Scale, dorsal surface uppermost in K, N, P – Q.

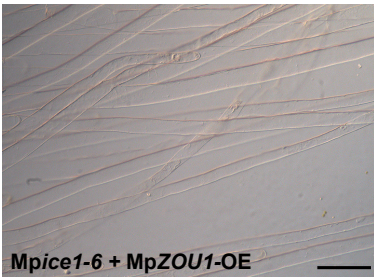
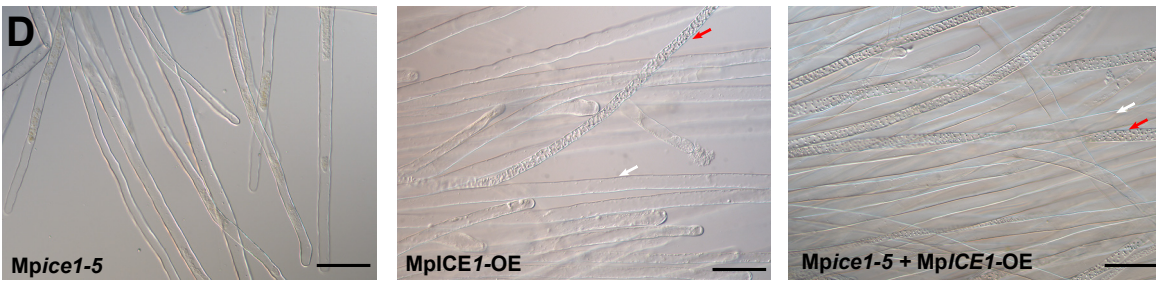
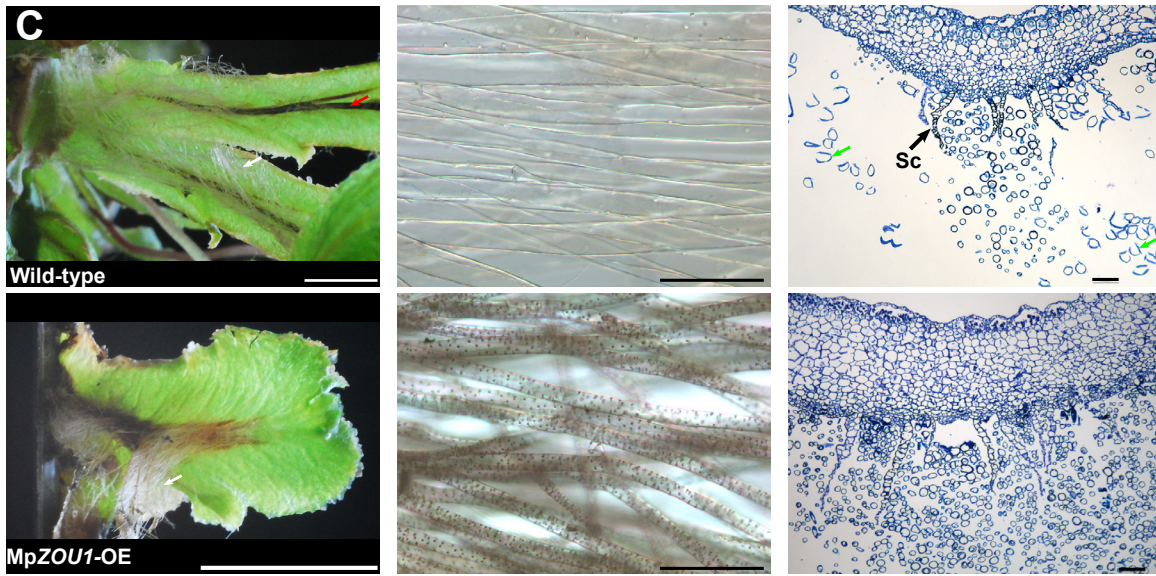
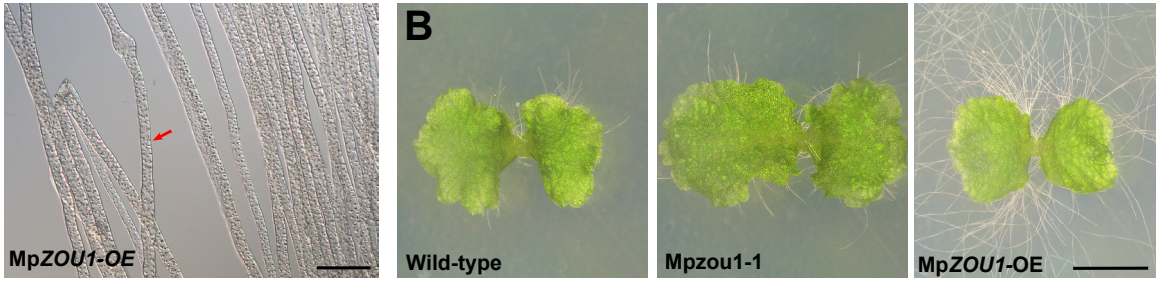
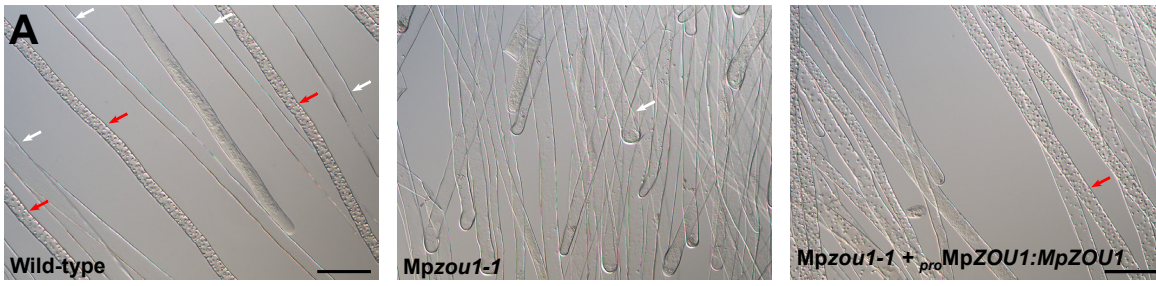


**Figure 4. MpZOU1 and MpICE1 promote pegged rhizoid formation**

(A) Light micrographs (DIC) of rhizoids of 12 day old gemmalings of wild type (Tak2), loss of function mutants, a complemented *Mpzou1* mutant and *MpZOU1*-OE. In wild type, pegged rhizoids are indicated with red arrows, smooth rhizoids with white arrows. Smooth rhizoids typically have slightly wider bore than pegged. Scale bar 100  $\mu$ M (B) Like wild-type (Tak1), rhizoids emerge from the ventral but not the dorsal epidermis of *MpZOU1*-OE. Scale bar 1mm (C) Ventral surface of ten week old thallus of wild type and *MpZOU1*-OE (left panel). In wild type, bundles of pegged rhizoids are covered with red pigmented scales and grow parallel to thallus surface along the midrib (red arrow). Smooth rhizoids emerge outside the scales and grow away from the epidermis (white arrow), scale bar 1cm. DIC microscopy (middle panel, scale bar 100  $\mu$ M) on the latter confirm that they are smooth rhizoids. Transverse sections through the midrib region (right panel, scale bar 100  $\mu$ M) show pegged rhizoids under scales (Sc) at the midrib and larger, lighter staining smooth rhizoids (green arrows) towards the periphery. In *MpZOU1*-OE the rhizoids growing away from the thallus are all pegged (middle and right panels). (D) Light micrographs (DIC) of 12 day old gemmalings of *Mpice1* mutant and *MpICE1*-OE in wild type and *Mpice1* mutant backgrounds. *MpICE1* OE complements the *Mpice1* mutant phenotype, whereas *MpZOU1* OE does not. Scale bar 100  $\mu$ M



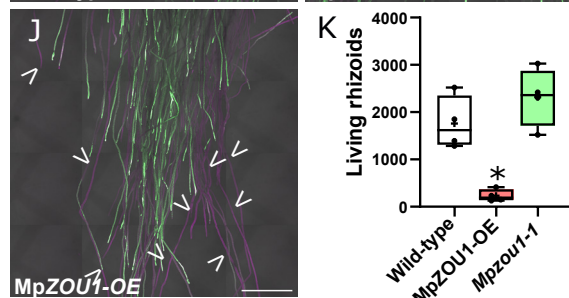
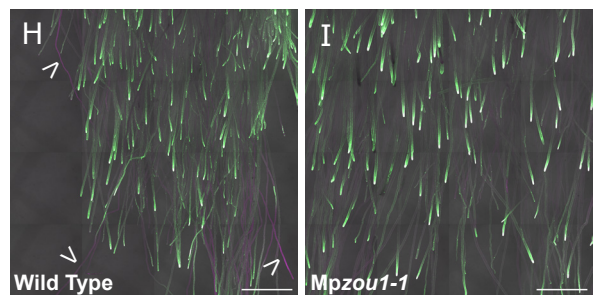
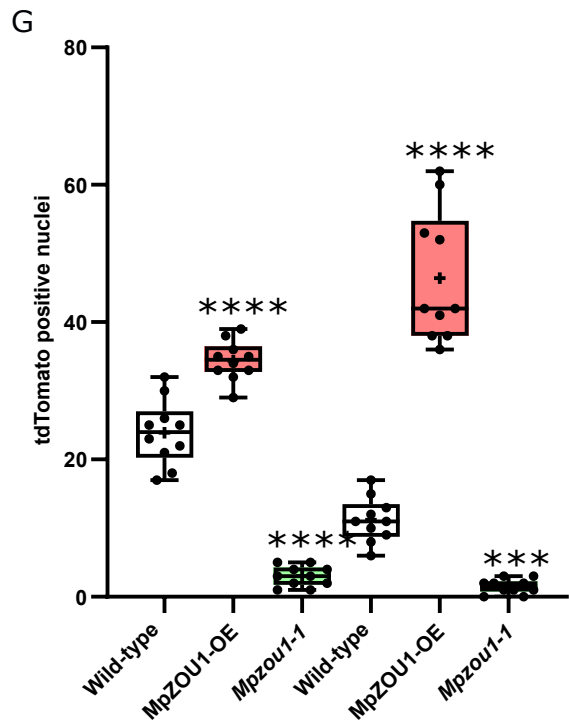
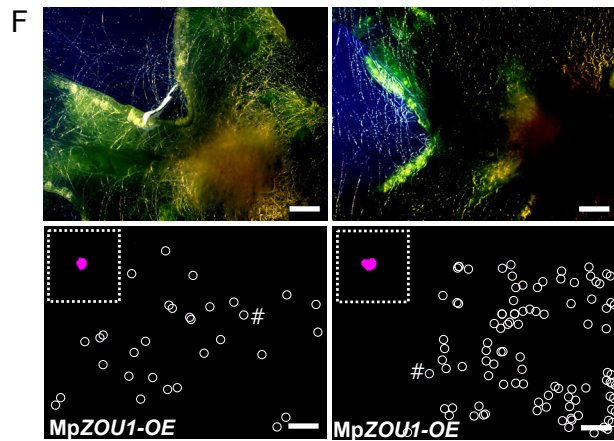
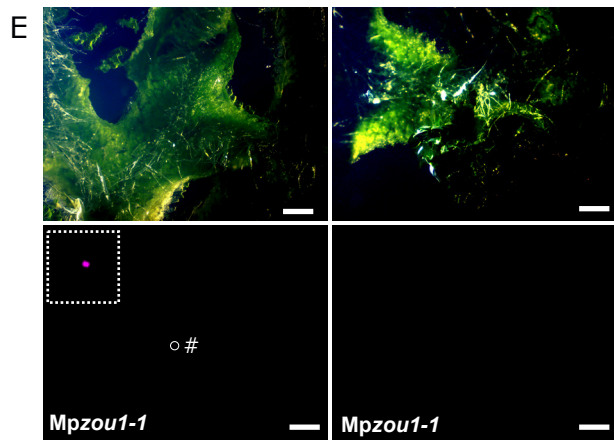
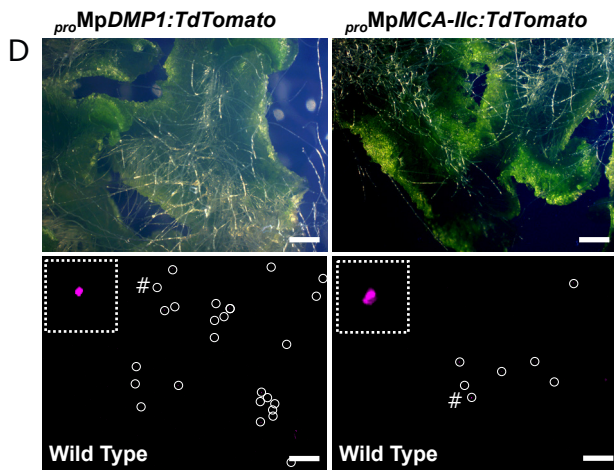
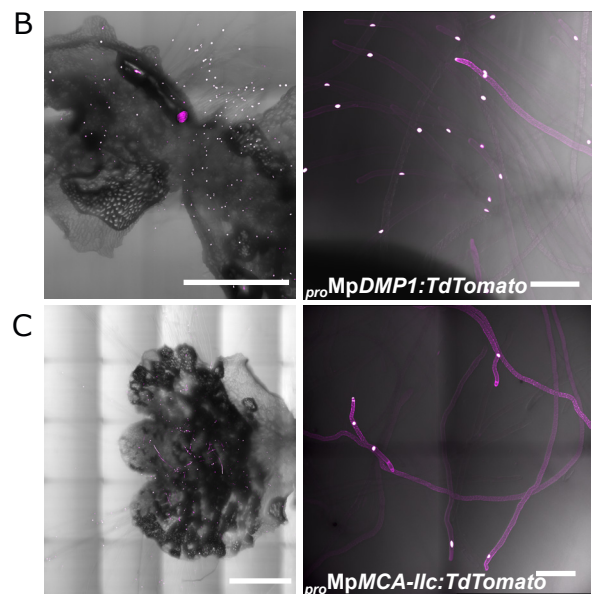
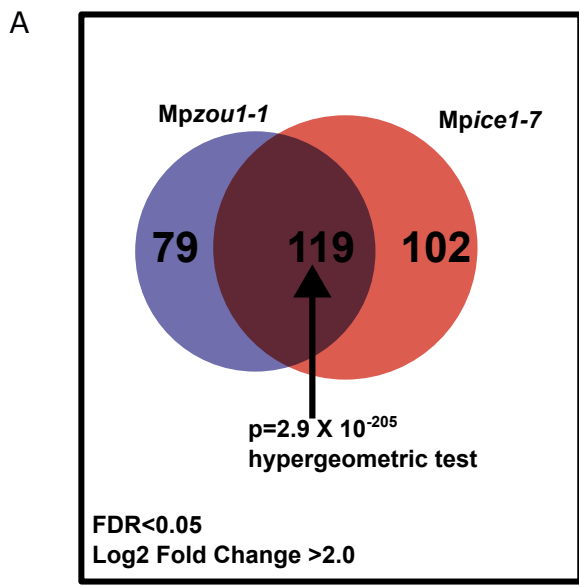


**Figure 5. MpZOU1 controls pegged rhizoid programmed cell death**

(A) Expression of orthologues of dPCD-associated genes.

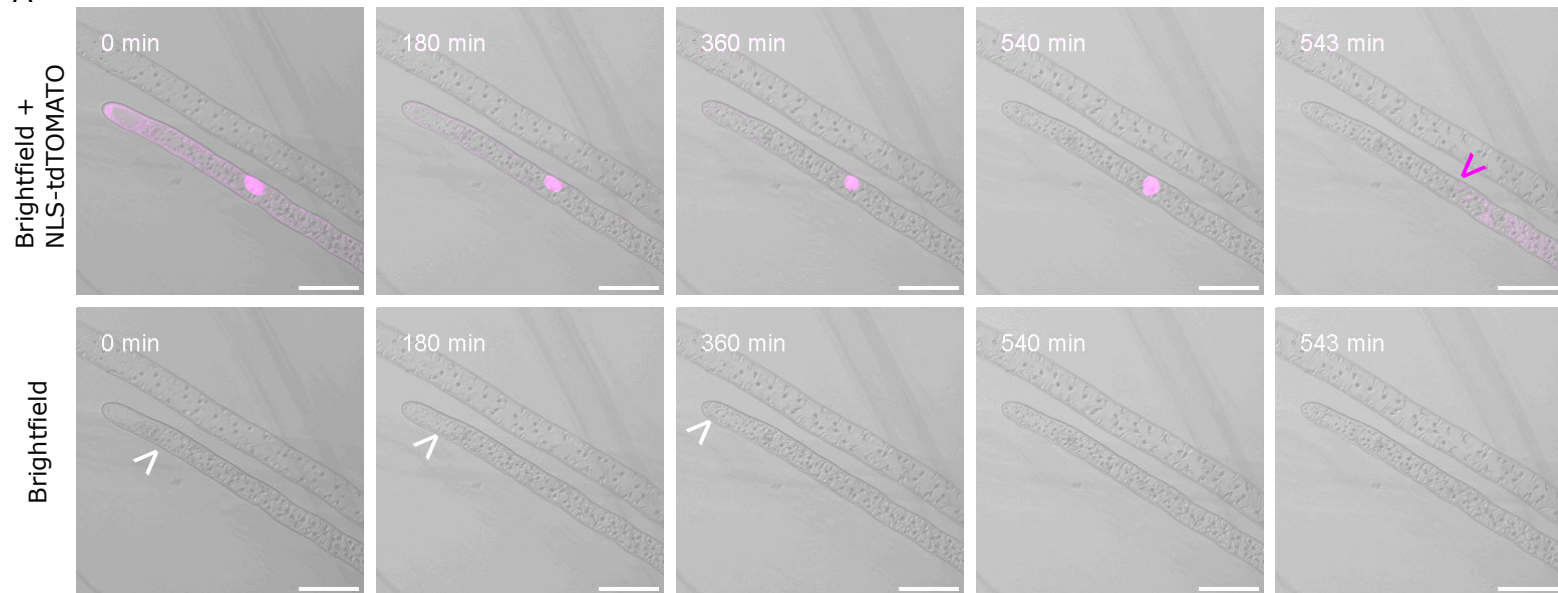
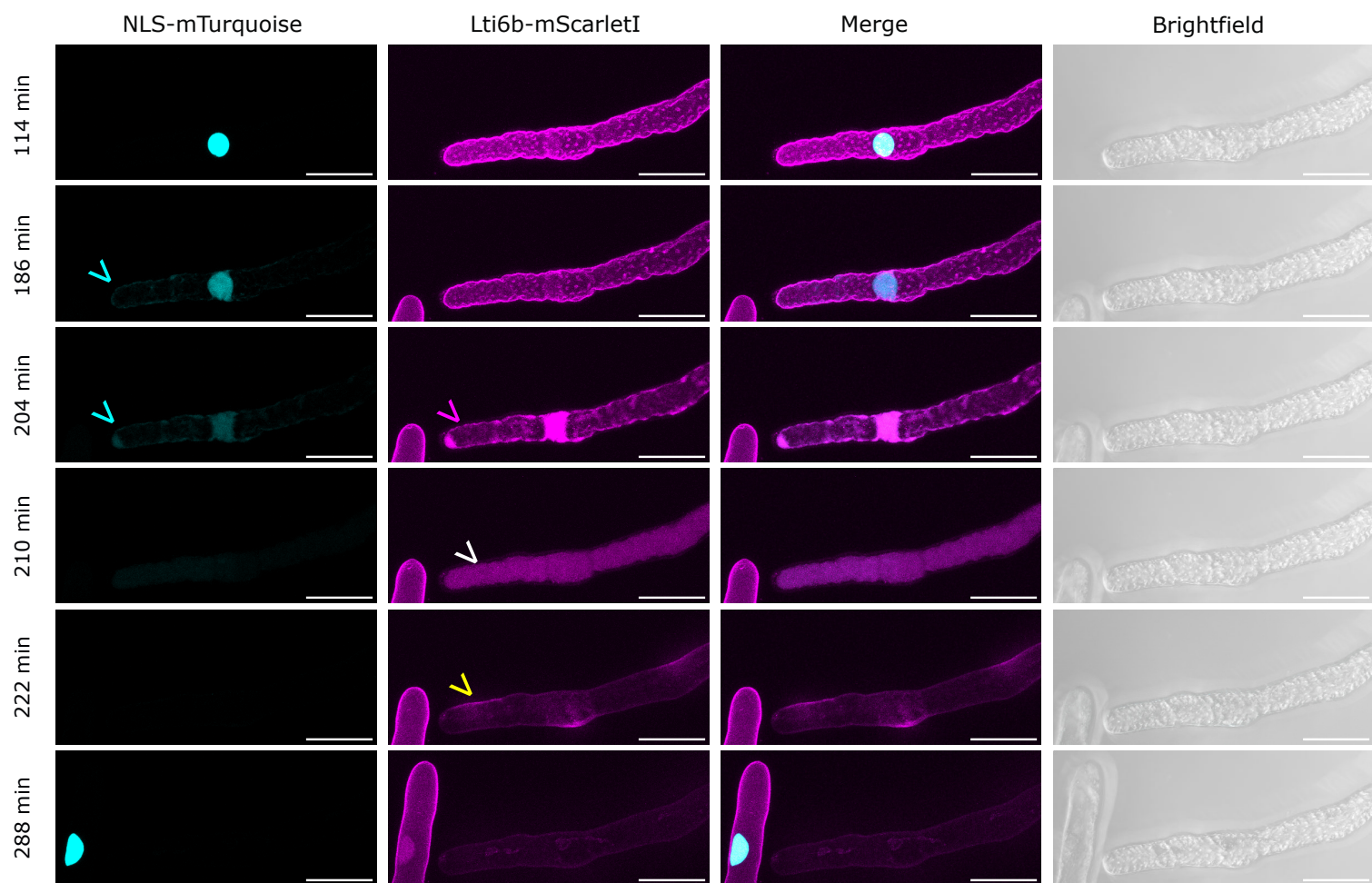
(B-C) Expression pattern of *pro*MpDMP1 (B) and *pro*MpMCA-*Ilc* transcriptional reporters (C) in wild-type (Tak1) 2-week old thalli (left panels) and rhizoids (right panels). Bars 1mm (right panels) ; 100µm (left panels).

(D-F) Expression pattern of *pro*MpDMP1 (left panel) and *pro*MpMCA-*Ilc* (right panel) in wild-type (Tak1) (D), *Mpzou1-1* (E) and MpZOU1-OE (F) in 6-week old thalli. Bar 2mm. White circles indicate visible nuclei, hashtag indicates the nucleus in the inset.

(G) Number of tdTomato nuclei observed in 6 weeks old thalli of PCD reporter lines in wild-type (Tak1), MpZOU1-OE and *Mpzou1-1* genotypes. n=10, ordinary one-way ANOVA \*\*\*P-value<0.001 ; \*\*\*\* P-value<0.0001

(H-J) Confocal tiling images of FDA-PI stained rhizoids of 19-day old thalli. Dead (PI-positive, FDA-negative) rhizoids are indicated by arrowheads in wild-type (Tak1) (H) and MpZOU1-OE (J), but are absent in *Mpzou1-1* (I). Scale bar, 1mm.

(K) Quantification of nuclear foci in wild-type (Tak1), *Mpzou1-1*, and MpZOU1-OE in substrate rhizoids at 19-day old thalli indicating more nuclei in *Mpzou1-1*, and less in MpZOU1-OE when compared to wild type. n=4, Mann Whitney test \*P-value<0.05.

**A****B**

**Figure 6. Terminal differentiation of pegged rhizoids ends with cell death**

(A) Confocal time-lapse imaging of a pegged rhizoid expressing *proMpZOU1:tdTomato-NLS*. Time indicated in minutes (min) corresponding to Video S2. The magenta arrowhead marks the first time frame after nuclear envelope breakdown, the white arrowheads marks the advancing front of peg formation reaching the tip of the rhizoid prior to cell death execution. (B) Confocal time-lapse imaging of a pegged and a smooth rhizoid expressing a double reporter (nuclear *proMpUBE2:mTurquoise-N7* [cyan], plasma membrane-bound *proMpUBE2:ScarletI-Lti6b* [magenta]). Time indicated in minutes (min) corresponding to Video S1. The cyan arrowhead marks leakage of nuclear mTurquoise-N7 into the cytosol indicating nuclear envelope breakdown. Magenta arrowhead marks solubilization of ScarletI-Lti6b into the cytosol, indicating endodomain shedding. White arrowhead marks even distribution of ScarletI-Lti6b in the cell lumen, indicating vacuolar collapse. Yellow arrowhead marks leakage of ScarletI-Lti6b into the extracellular space indicating plasma membrane disintegration. Scale bars are 50 $\mu$ m.

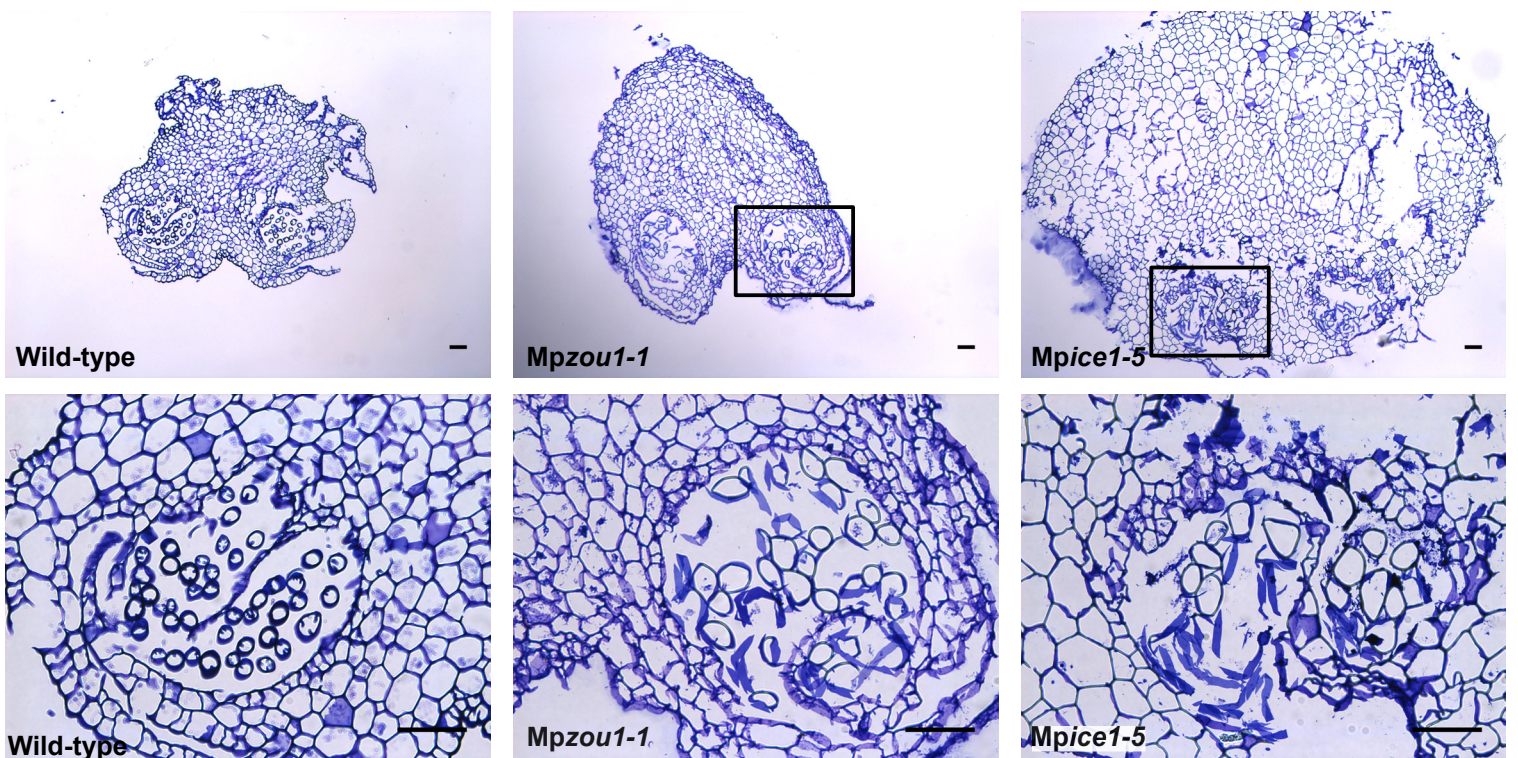
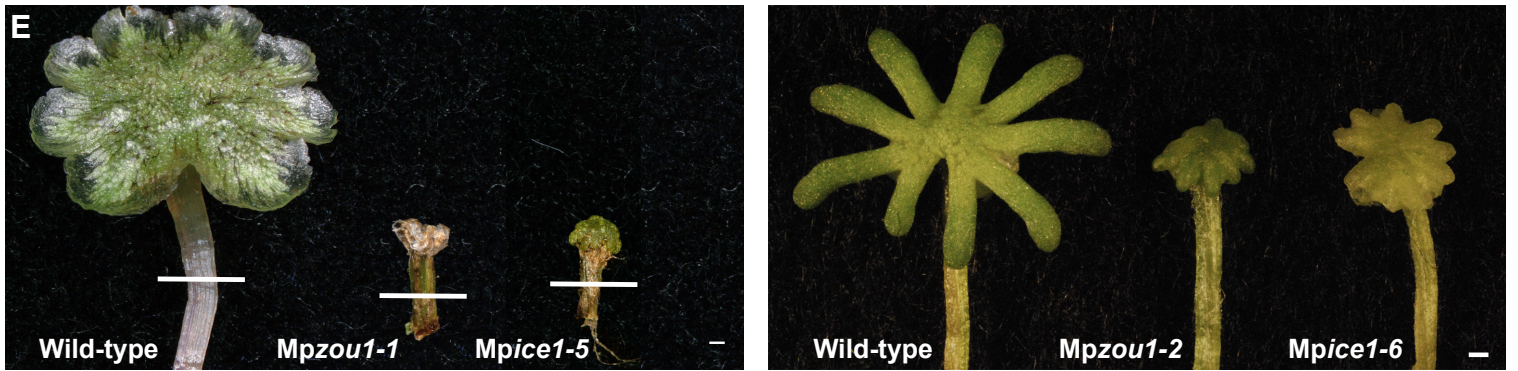
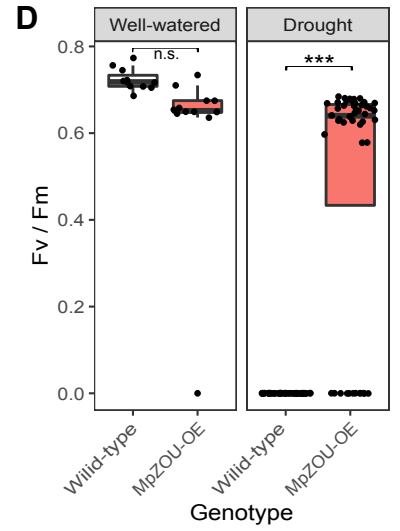
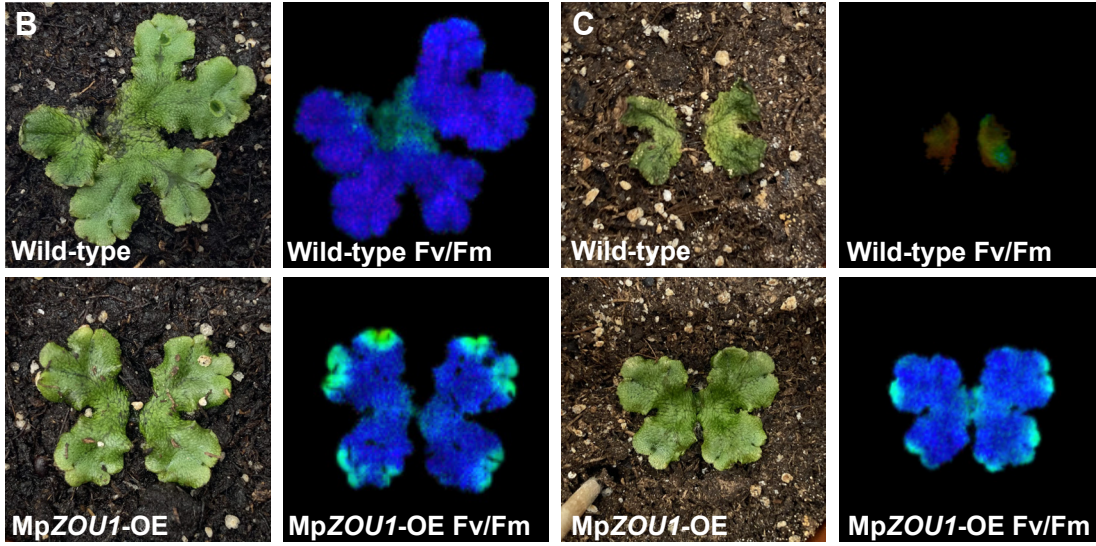
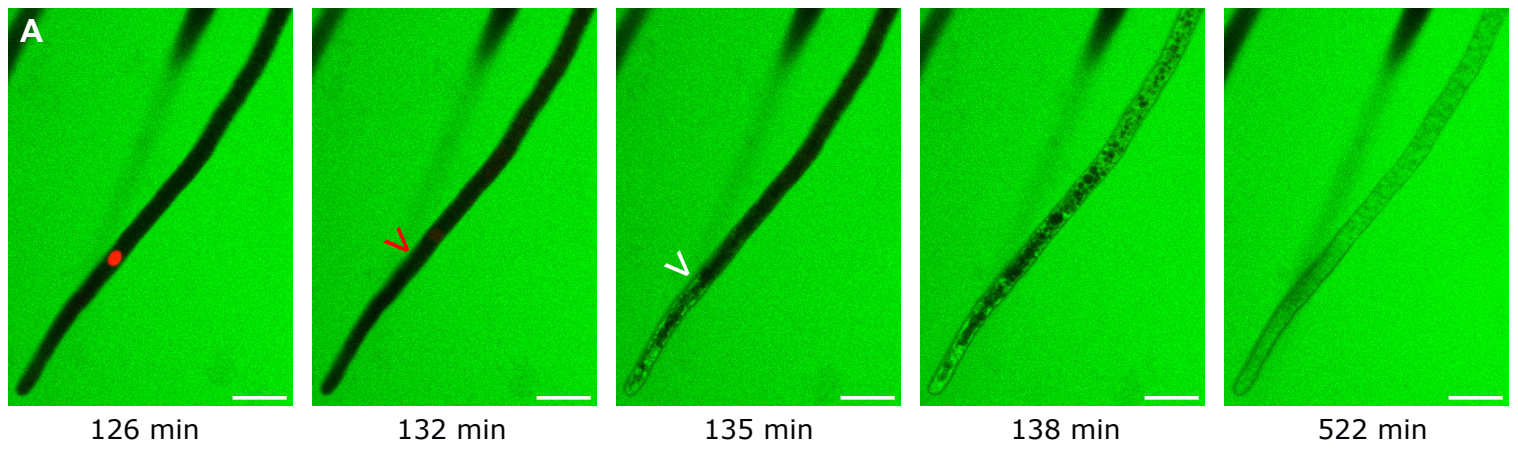


**Figure 7. MpZOU1 and MpICE1 promote water uptake**

- (A) Confocal time lapse imaging of a pegged rhizoid expressing *proMpZOU1:tdTomato-NLS* (red signal). Red arrowhead marks nuclear envelope breakdown, followed by a diffusion of the non-membrane permeable fluorescein (green signal) into the lumen, indicating failure of plasma-membrane integrity (white arrowhead). Scale bars are 50 $\mu$ m.
- (B) Representative images of wild type (Tak1) and MpZOU1-OE thalli under well-watered conditions, regular photo on the right, Fv/Fm ratiometric image on the left.
- (C) Representative images of wild type (Tak1) and MpZOU1-OE thalli under well-watered conditions, regular photo on the right, Fv/Fm ratiometric image on the left. Images in B) and C) are 25 mm wide.
- (D) Quantification of Fv/Fm measurements in well-watered and drought-stressed thalli of Tak1 wild type and MpZOU1-OE. A Welch's two-sample t-tests indicates a non-significant (n.s.) PSII photochemical efficiency in well-watered conditions ( $p = 0.07225$ ), but a highly significant difference in PSII photochemical efficiency in MpZOU1-OE under drought conditions (\*\*\*,  $p = 1.063e-15$ ).
- (E) Gametophores of mutant lines are smaller than wild type and frequently desiccated (upper panel). The white lines indicate approximate position of the transverse sections of wax embedded stalks shown in the lower panels. Two bundles of internalized pegged rhizoids run up the stalks (arrows in middle row). In wild type all rhizoids are pegged, in the mutants there are fewer rhizoids and they are smooth, slightly wider in bore and lighter staining than pegged rhizoids as seen in high magnification images (bottom row). Scale bars are 500  $\mu$ M in upper panel and 50  $\mu$ M in lower panels.

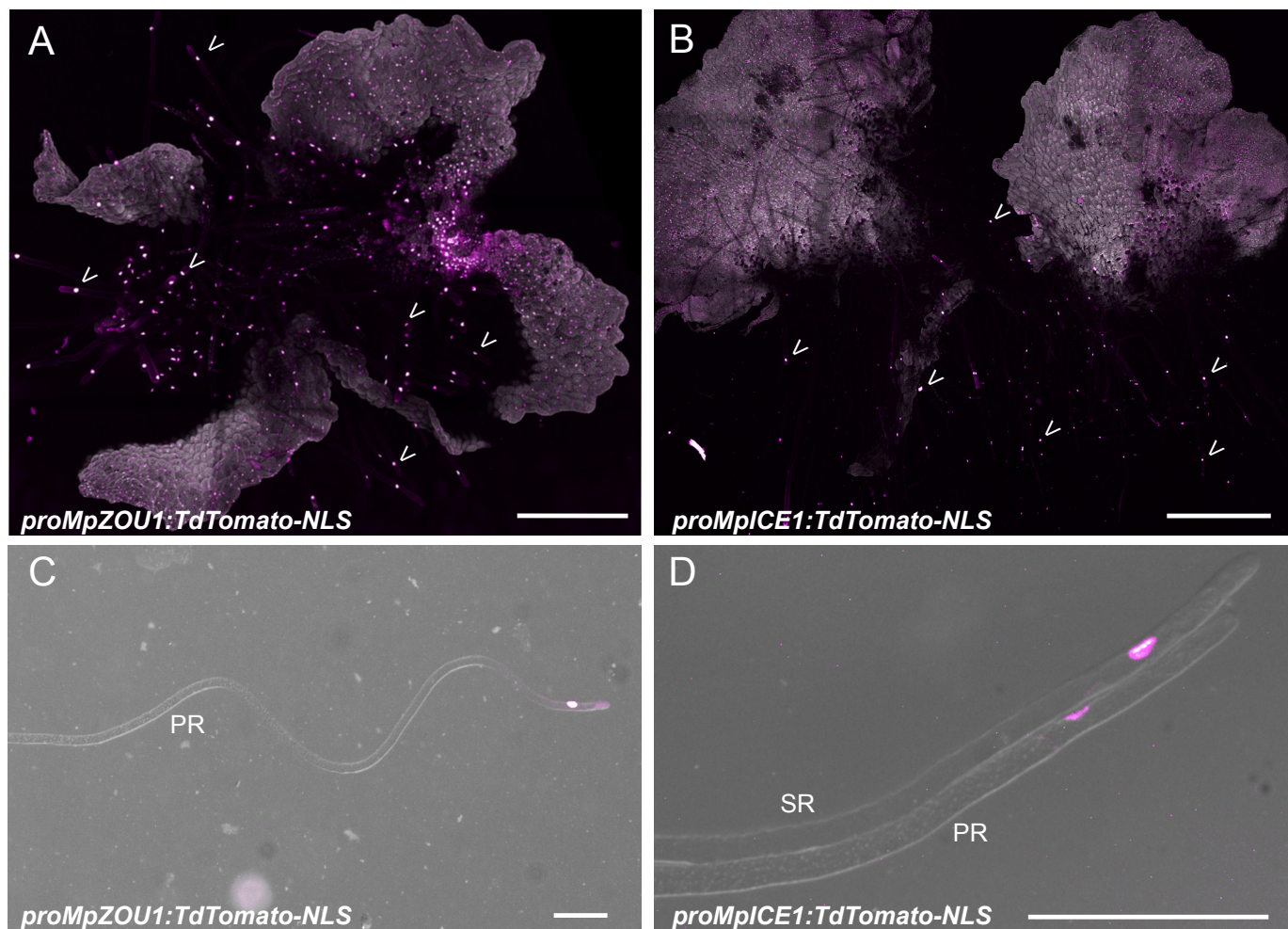
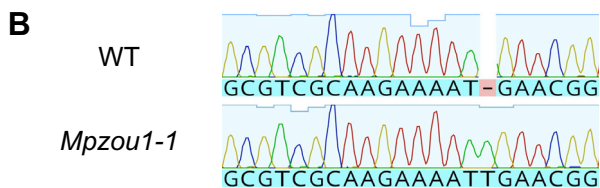
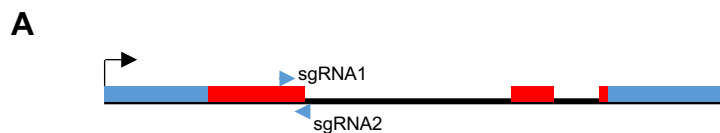


**Figure S1 The *MpZOU1* and *MpICE1* genes are expressed in rhizoids.**

(A-B) Confocal composite images of maximum Z-stack projections showing fluorescence of nuclear localized *proMpZOU1:NLS-TdTomato* (A) and *proMpICE1:NLS-TdTomato* (B) transcriptional reporter constructs. Expression can be seen in the underside of the thalli and in growing rhizoids (isolated nuclei, some indicated by arrowheads).

(C-D) Higher-resolution confocal images of *proMpZOU1:NLS-TdTomato* (C) and *proMpICE1:NLS-TdTomato* (D) overlaid with a transmitted light image showing expression in pegged rhizoids (PR) and a smooth rhizoid (SR), which could also be an immature pegged rhizoid. Scale bars are 1mm (A-B) or 0.2mm (C-D)



**C**

WT 5' -GCGTCGCAAGAAAA-**TGAACGG**-3'

*Mpzou1-1* 5' -GCGTCGCAAGAAAA**T**TGAACGG-3' (+1bp)

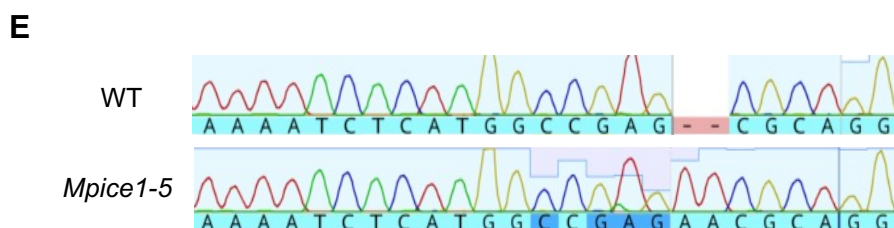
*Mpzou1-5* 5' -GCGTCGCAAGAAAA**T**TGAACGG-3' (+1bp)

WT 5' -GCGTCGCAAGAAAATG-----**AA**CGG-3'

*Mpzou1-6* 5' -GCGTCGCAAGAAAATG**TTCTCCACGTT**-ACGG-3' (+11bp -1bp = +10bp)

WT 5' -ATCACCTTGGAGTTGAGA**TGG**-3'

*Mpzou1-2* 5' -ATCACCTTG-----GAGATGG-3' (-5bp)



**F**

WT 5' -AAAATCTCATGGCCGA-----**GCGC**AGG-3'

*Mpice1-2* 5' -AAAATCTCATGGCCGA**AAAATTCT**GCGCAGG-3' (+8bp)

WT 5' -AAAATCTCATGGCCGAG--**CGC**AGG-3'

*Mpice1-4* 5' -AAAATCTCATGGCCGAG**T**-CGCAGG-3' (+1bp)

*Mpice1-5* 5' -AAAATCTCATGGCCGAG**AA**CGCAGG-3' (+2bp)

*Mpice1-7* 5' -AAAATCTCATGGCCGAG**A**-CGCAGG-3' (+1bp)

WT 5' -AAAATCTCA-----TGGCCGAGCGC**AGG**-3'

*Mpice1-6* 5' -AAAATCTCA**GATTCATAAAAATGAGATTCATAAAAATCTCAT**-----CGC**AGG**-3'

(+32bp -8bp = +24bp)

**Figure S2. Mpzou1 and Mpice1 mutant alleles produced by genome editing**

A. Schematic of MpZOU1 gene, filled rectangles indicate exons, untranslated regions are shown in blue and coding sequences in red. sgRNA1 and 2 target basic and loop regions of bHLH domain, respectively. B. Chromatograms showing sequence alteration in *Mpzou1-1* allele. C. Sequence of *Mpzou1* alleles. The sgRNA sequence is underlined in wild type (WT) and the PAM sequence shown in bold. *Mpzou1-1* and *Mpzou1-5* have the same lesion but were independent isolates. The alleles were generated with sgRNA1 except *Mpzou1-2* which was from sgRNA2. D. Schematic of MpICE1 gene, sgRNA targets basic region of bHLH domain. E. Sequence of *Mpice1* alleles. The insertion in *Mpice1-6* introduces premature stop codons.



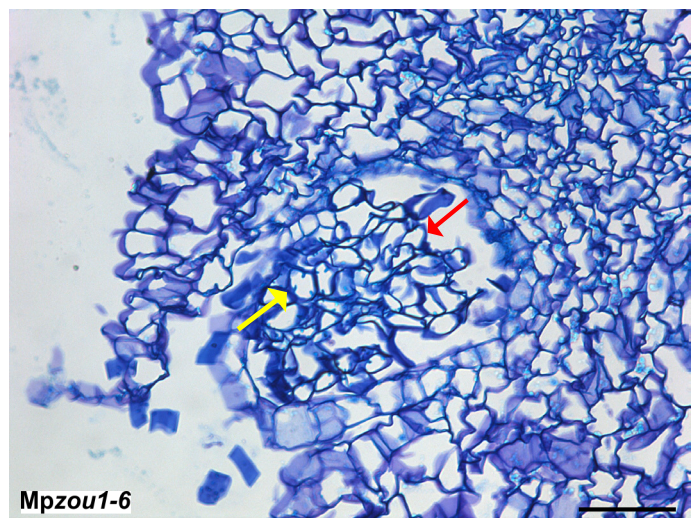
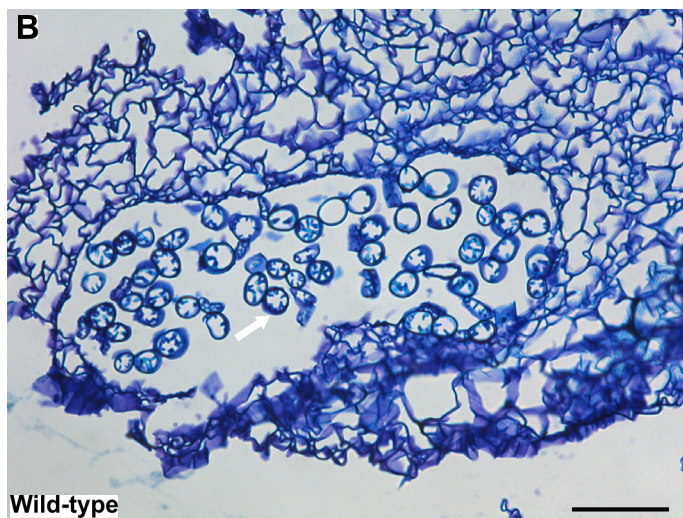
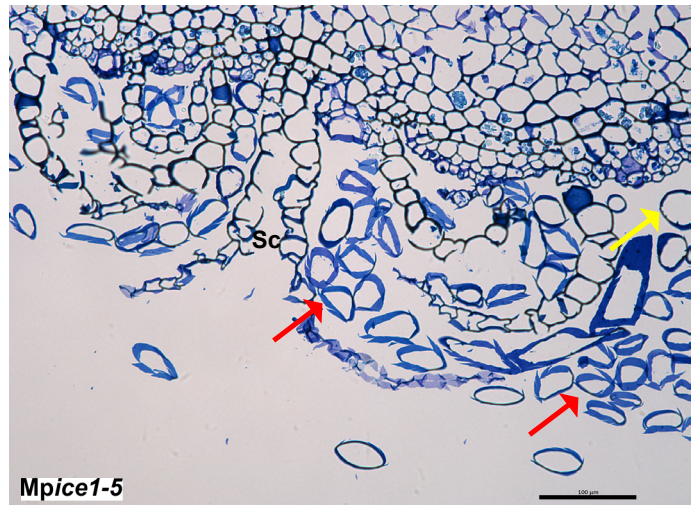
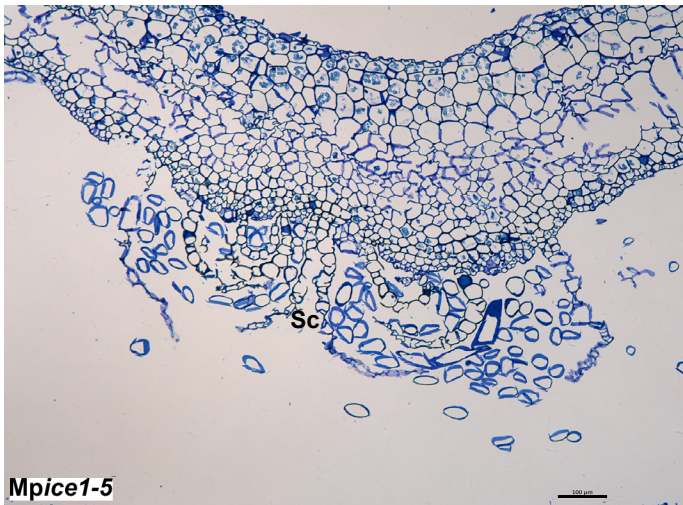
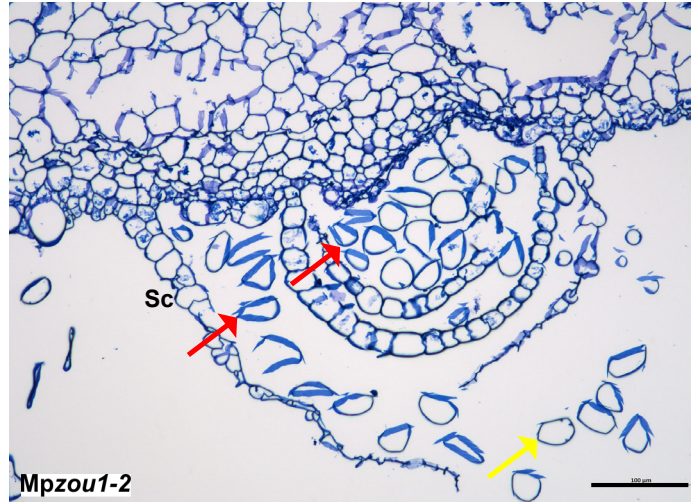
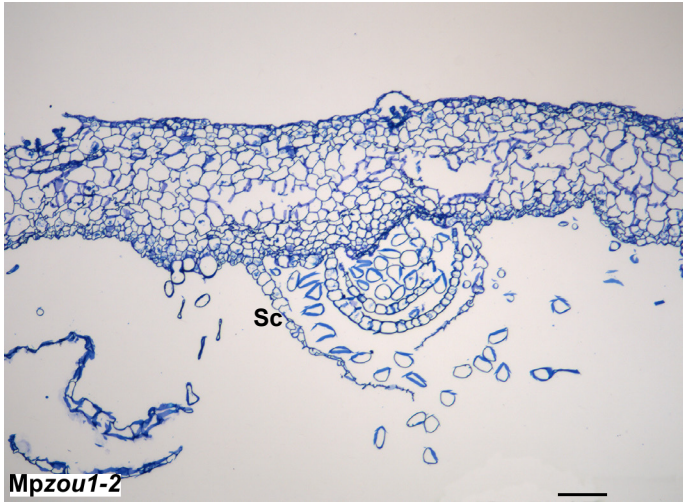
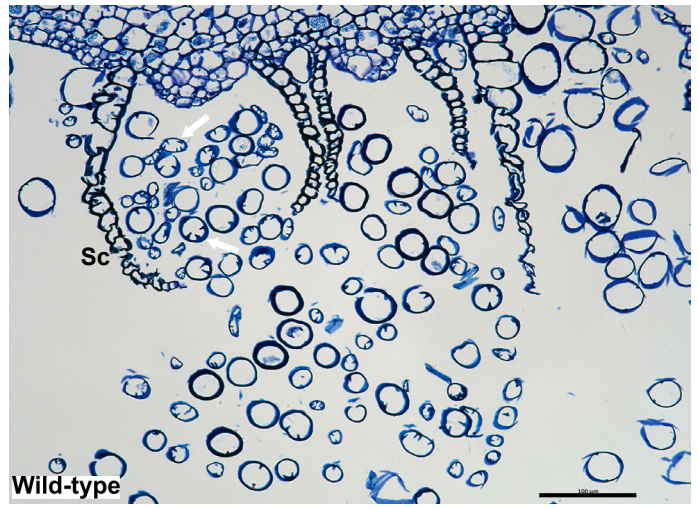
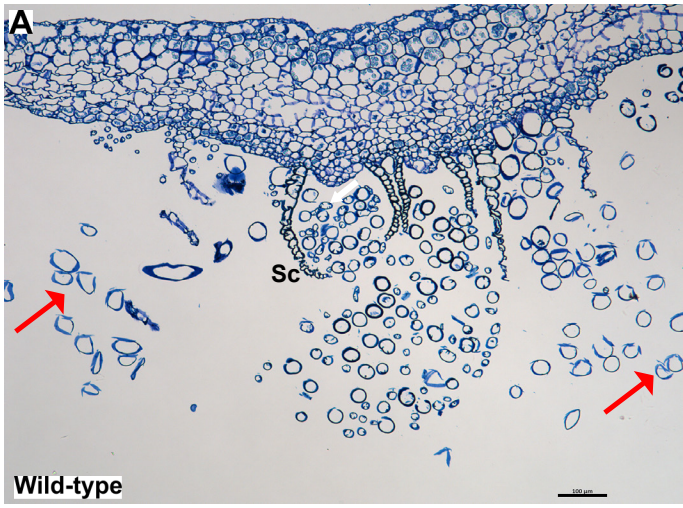


**Figure S3. Rhizoid formation in *Mpzou1* and *Mpice1* mutants.**

(A) Light micrographs of Toluidine Blue stained transverse sections of wax embedded midrib region of thallus of wild type and mutants. The right hand panels are higher magnification images of the sections in left hand panels. In wild type (Tak2) the smooth rhizoids are at the periphery of the sections and are slightly larger in bore and lighter staining than the pegged rhizoids, which are mainly in bundles under the scales (Sc) at the midrib. In the mutants, smooth rhizoids (note lighter staining and wider bore) replace pegged rhizoids in midrib region. Yellow arrows indicate rhizoids with partial peg formation in mutants. (B) Light micrographs of Toluidine Blue stained transverse sections of resin embedded antheriodophore stalks of wild type and *Mpzou1-6* mutant. White arrow indicates a pegged rhizoid in one of the two grooves of pegged rhizoids that run up the stalks. In the mutant, several rhizoids have pegs (yellow arrow) but they are much shorter than in wild type. Red arrows smooth rhizoids, white arrows pegged rhizoids, yellow arrows rhizoids with partially developed pegs. Scale bars 100  $\mu$ M

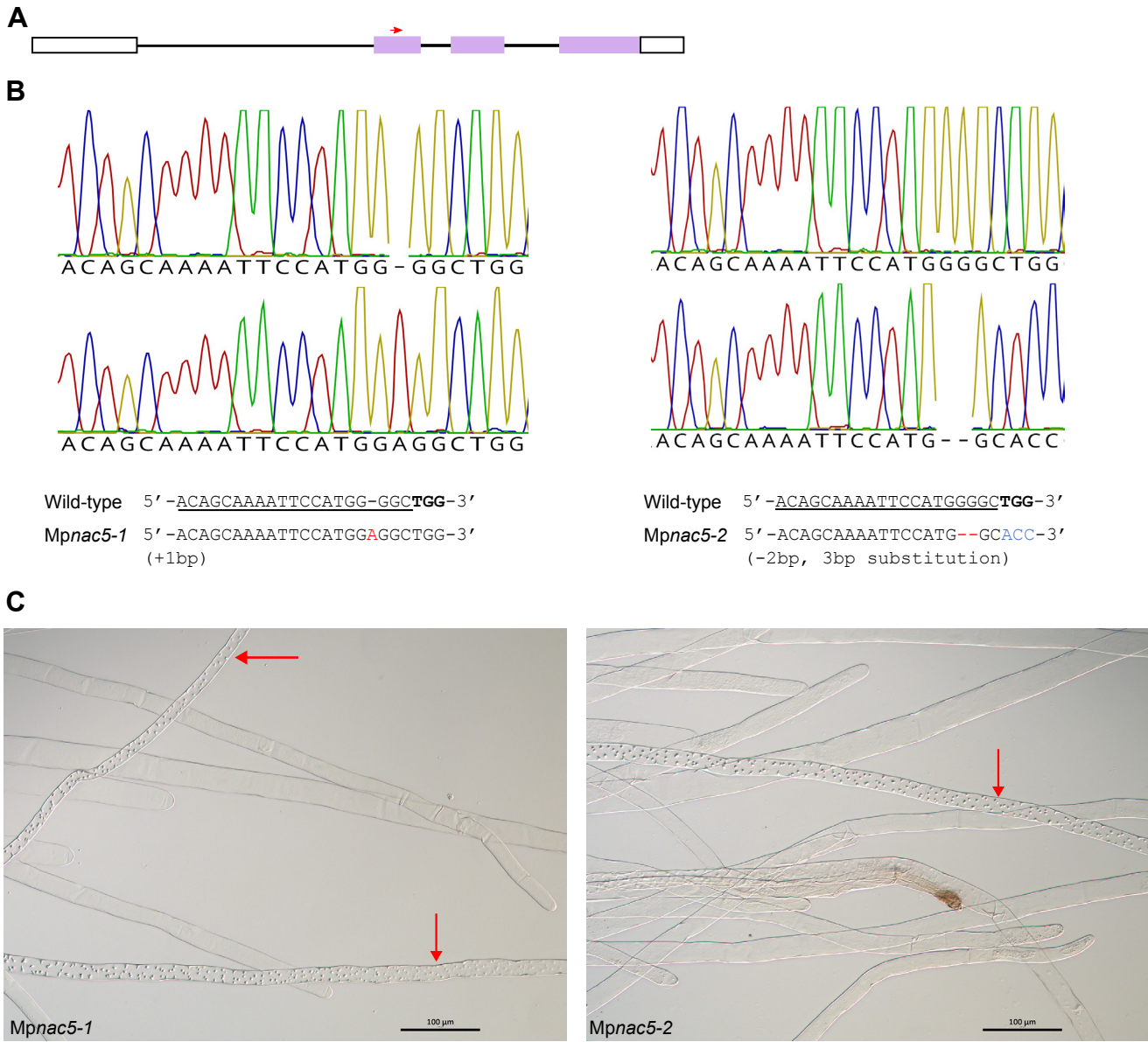


**Figure S4. Effect of MpNAC5 on pegged rhizoid development**

(A) Schematic of MpNAC5 (Mp6g20920) gene structure. Exons shown as boxes, introns as lines, coding sequences are coloured. Red arrow indicates position of sgRNA used for editing.

(B). Sequence chromatograms and alignments for two mutant alleles obtained. Bold indicates PAM sequence, sgRNA sequence is underlined, indels are in red, substitutions in blue. Both alleles introduce frameshifts and premature termination of translation and are likely nulls.

(C). Light micrographs of rhizoids from 7 day old mutant plants, pegged rhizoids indicated with red arrows. Scale bars 100μM

**Figure S5. Effects of *Mpzou1-1* and *MpZOU1*-OE on numbers of living rhizoids in thalli**  
(A-C) Confocal tile scans of Tak1, *Mpzou1-1*, and *MpZOU1*-OE rhizoids expressing nuclear localized mTurquoise and plasma-membrane localized mScarlet-I (*proMpUBE2:mTurquoise-N7, proMpUBE2:ScarletI-Lti6b*). Imaging of 19-day old thalli in that have been cultivated in microscopic chambers on agar. The substrate rhizoids grow through the agar and along the chamber bottom allowing convenient imaging from below. A) Wild-type (Tak1). B) *Mpzou1-1*. C) *MpZOU1*-OE. Inset shows a single tile at higher magnification, dashed squares indicate the location of the tile that is shown in the insets. Scale bars are 1mm, 100 $\mu$ m in the insets.

**A**

| Genotype  | Number of pegged rhizoids |
|---|---------------------------|
| Tak 1   | 5.9 ± 1.4                 |
| Tak 2   | 54.3 ± 5.2                |
| <i>Mpzou1-1</i>                                 | 0 ± 0                     |
| <i>Mpzou1-1</i> <i>pro</i> MpZOU1:MpZOU1 CDS #5 | 48.3 ± 3.9                |
| <i>Mpzou1-2</i>                                 | 0 ± 0                     |
| <i>Mpzou1-6</i>                                 | 0 ± 0                     |
| <i>Mpice1-5</i>                                 | 0 ± 0                     |
| <i>Mpice1-6</i>                                 | 0 ± 0                     |

**B**

| Genotype         | Rhizoid diameter (μm) | Range (μm)  | Significance group |
|------------------|-----------------------|-------------|--------------------|
| Wild type Smooth | 29.3 ± 0.8            | 22.6 – 40.6 | a                  |
| <i>Mpzou1-1</i>  | 26.5 ± 1.0            | 17.4 – 40.3 | a                  |
| <i>Mpice1-5</i>  | 25.9 ± 0.5            | 18.2 – 32.9 | a                  |
| Wild type Pegged | 19.0 ± 0.6            | 12.7 – 23.5 | b                  |
| MpZOU1 OE        | 18.2 ± 0.4            | 12.5 – 25.3 | b                  |

**Table S1. MpZOU1 and MpICE1 control pegged rhizoid formation**

(A) Mean number of pegged rhizoids, ± standard error of mean (n=9-10), in 12 day old gemmalings.

(B) Mean diameter of rhizoids, ± standard error of mean (n>23) in 12 day old gemmalings, measured from DIC micrographs of whole mount fresh tissue. For wild type (Tak2), rhizoids with pegs were measured separately from those lacking pegs (i.e. mainly smooth with a few pegged pre-differentiation). Statistical analysis (ANOVA followed by Dunn's post hoc test Bonferoni corrected) indicated significant differences ( $p < 0.01$ ) between groups a and b but not within the two groups.

**Table S2 Cell wall, cell death and redox genes are down-regulated in *Mpzou1* and *Mpice1* mutants.** Selected genes down-regulated in both *Mpzou1* and *Mpice1* mutants are shown together with the log2 fold change values.

| Gene ID                       | Annotation                       | L <sub>2</sub> FC <i>Mpzou1</i> /WT | L <sub>2</sub> FC <i>Mpice1</i> /WT |
|-------------------------------|----------------------------------|-------------------------------------|-------------------------------------|
| <b>Cell Wall Modification</b> |                                  |                                     |                                     |
| <i>Mp4g03640</i>              | D-mannose binding lectin protein | -7.31                               | -8.69                               |
| <i>Mp3g06900</i>              | Expansin                         | -3.33                               | -6.17                               |
| <i>Mp5g22020</i>              | FASCICLIN-like arabinogalactan 2 | -5.38                               | -2.69                               |
| <i>Mp8g02360</i>              | Proline rich extensin signature  | -3.19                               | -5.65                               |
| <i>Mp3g03160</i>              | Rhamnogalacturonan endolyase     | -8.80                               | -8.10                               |
| <i>Mp2g13580</i>              | Rhamnogalacturonan endolyase     | -8.60                               | -8.70                               |
| <i>Mp2g13570</i>              | Rhamnogalacturonan endolyase     | -8.20                               | -7.80                               |
| <i>Mp5g20220</i>              | Rhamnogalacturonan endolyase     | -5.89                               | -7.25                               |
| <i>Mp7g11130</i>              | Rhamnogalacturonan endolyase     | -3.85                               | -2.26                               |
| <i>Mp5g20220</i>              | Rhamnogalacturonan endolyase     | -5.89                               | -7.25                               |
| <i>Mp4g00700</i>              | Xyloglucan endotransglycosylase  | -9.80                               | -10.60                              |
| <i>Mp4g00680</i>              | Xyloglucan endotransglycosylase  | -7.84                               | -7.91                               |
| <i>Mp4g00670</i>              | Xyloglucan endotransglycosylase  | -6.05                               | -5.41                               |
| <i>Mp4g00690</i>              | Xyloglucan endotransglycosylase  | -5.69                               | -5.75                               |
| <i>Mp2g02380</i>              | Xyloglucan endotransglycosylase  | -5.33                               | -5.40                               |
| <b>Cell Death</b>             |                                  |                                     |                                     |
| <i>Mp8g07700</i>              | Metacaspase                      | -5.99                               | -4.34                               |
| <i>Mp6g12240</i>              | DUF679 containing DMP-like       | -8.53                               | -9.33                               |
| <i>Mp5g12180</i>              | DUF679 containing DMP-like       | -6.55                               | -7.53                               |
| <i>Mp5g12170</i>              | DUF679 containing DMP-like       | -4.57                               | -5.50                               |
| <i>Mp4g17600</i>              | DUF679 containing DMP-like       | -3.71                               | -5.02                               |
| <i>Mp4g17620</i>              | DUF679 containing DMP-like       | -2.17                               | -2.32                               |
| <i>Mp5g16420</i>              | Aspartyl protease                | -10.79                              | -9.57                               |
| <i>Mp5g16430</i>              | Aspartyl protease                | -9.37                               | -8.22                               |
| <i>Mp5g16410</i>              | Aspartyl protease                | -6.99                               | -7.06                               |
| <i>Mp5g12100</i>              | Aspartyl protease                | -5.92                               | -7.23                               |
| <i>Mp5g16350</i>              | Aspartyl protease                | -4.97                               | -5.23                               |

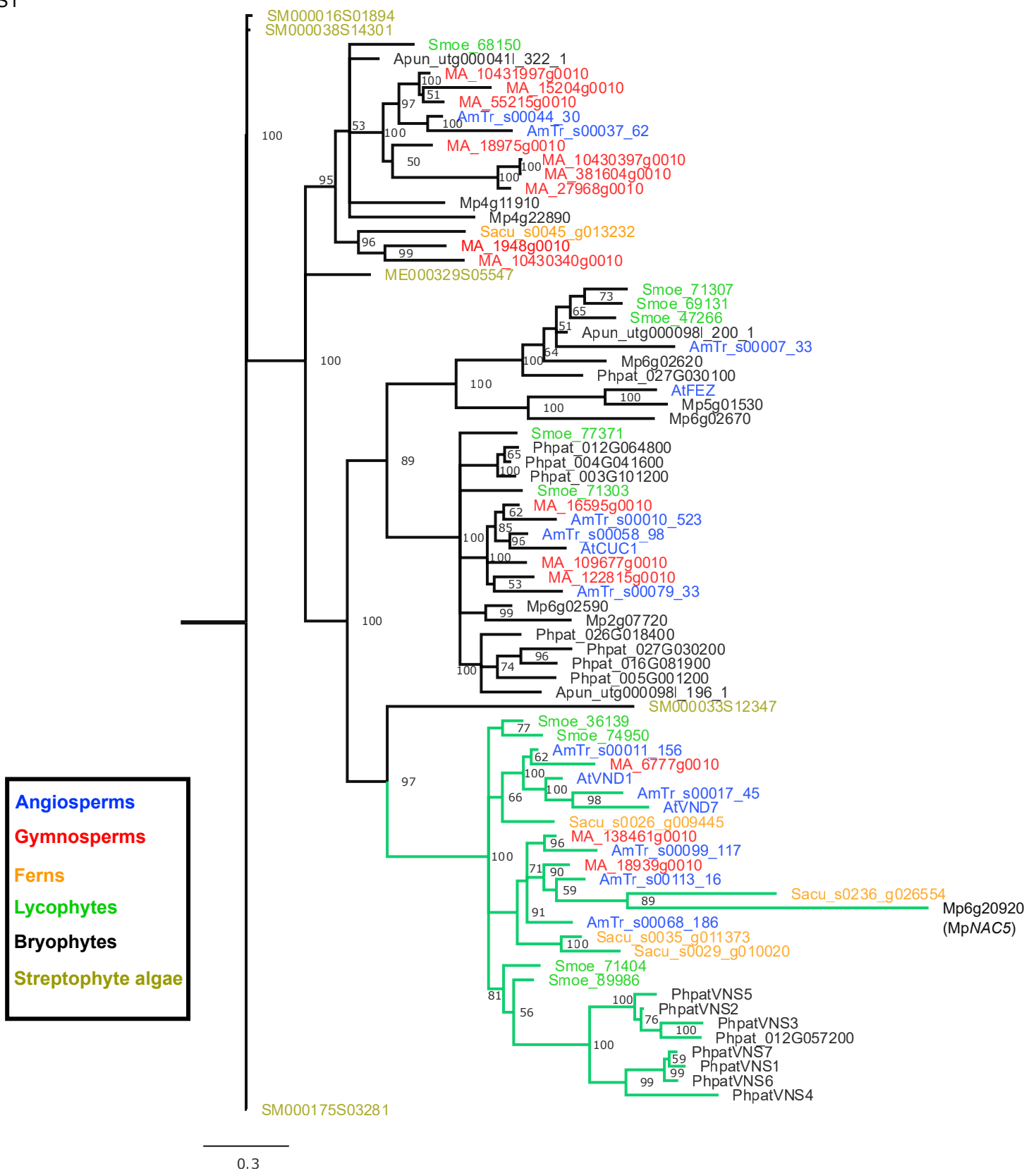
|                  |                            |       |       |
|------------------|----------------------------|-------|-------|
| <i>Mp5g12090</i> | Aspartyl protease          | -4.26 | -2.94 |
| <i>Mpzg01030</i> | ATP-dependent Clp protease | -3.09 | -3.14 |
| <i>Mp8g14580</i> | Metalloprotease            | -2.49 | -2.50 |
| <i>Mp8g01650</i> | Lipoxygenase               | -5.38 | -4.42 |
| <i>Mp8g15570</i> | Lipoxygenase               | -3.63 | -5.18 |

**Redox**

|                  |            |       |       |
|------------------|------------|-------|-------|
| <i>Mp5g06310</i> | Peroxidase | -9.88 | -6.51 |
| <i>Mp5g17080</i> | Peroxidase | -9.13 | -9.20 |
| <i>Mp5g17030</i> | Peroxidase | -8.90 | -3.42 |
| <i>Mp5g02520</i> | Peroxidase | -8.19 | -3.41 |
| <i>Mp5g17120</i> | Peroxidase | -8.16 | -8.23 |
| <i>Mp5g17130</i> | Peroxidase | -8.11 | -8.89 |
| <i>Mp5g17110</i> | Peroxidase | -7.06 | -7.06 |
| <i>Mp2g24530</i> | Peroxidase | -6.59 | -6.24 |
| <i>Mp6g21140</i> | Peroxidase | -5.79 | -5.85 |
| <i>Mp5g19410</i> | Peroxidase | -5.59 | -8.85 |
| <i>Mpzg01380</i> | Peroxidase | -5.24 | -6.03 |
| <i>Mp4g14270</i> | Peroxidase | -5.03 | -5.11 |
| <i>Mp5g09230</i> | Peroxidase | -4.51 | -4.34 |
| <i>Mp5g02600</i> | Peroxidase | -3.20 | -2.61 |
| <i>Mp1g22970</i> | Peroxidase | -3.02 | -4.26 |
| <i>Mp5g10750</i> | Peroxidase | -2.99 | -6.85 |
| <i>Mp5g06280</i> | Peroxidase | -2.47 | -3.12 |

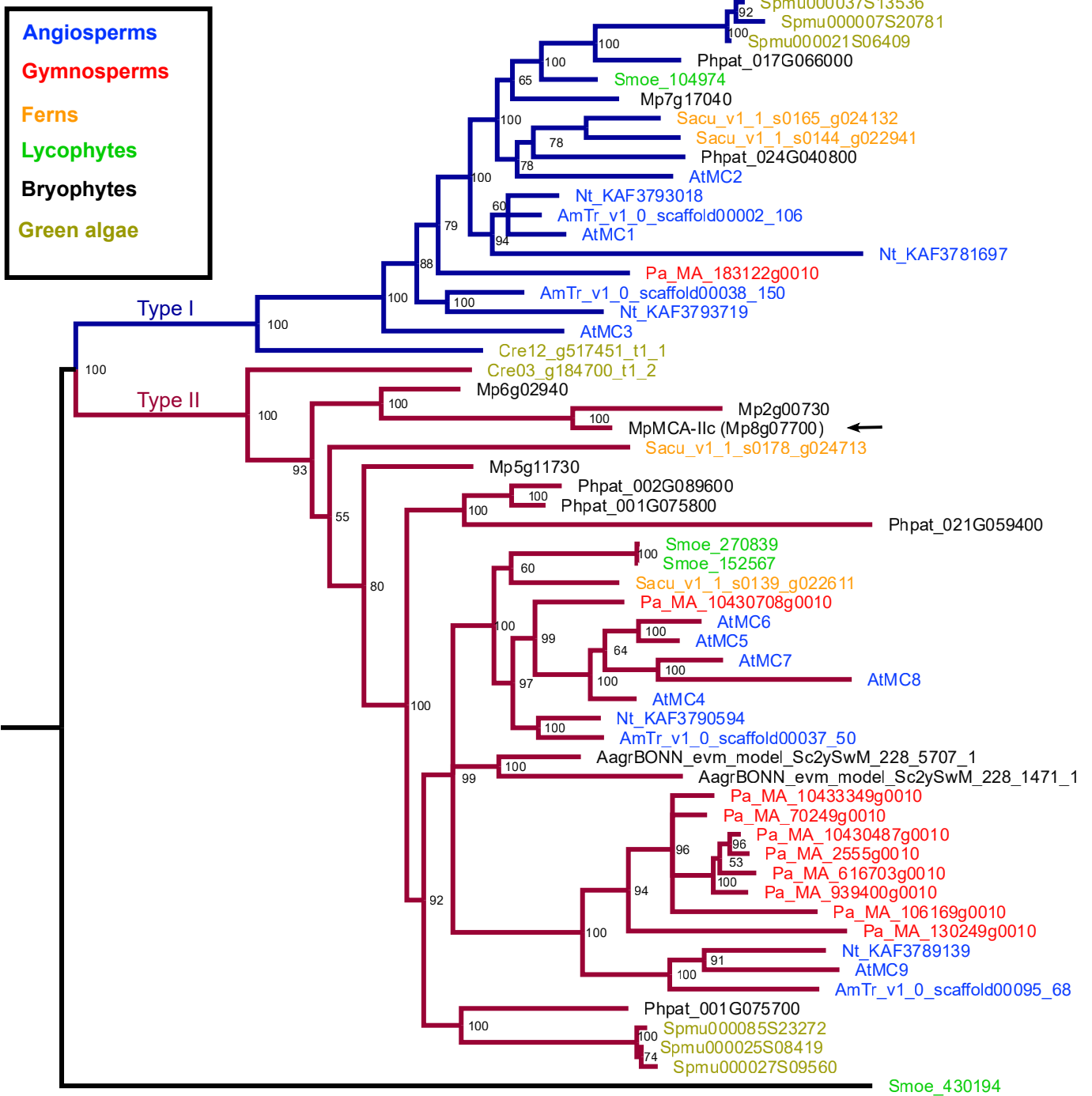
**Other**

|                  |                   |       |       |
|------------------|-------------------|-------|-------|
| <i>Mp4g03020</i> | Aquaporin         | -7.21 | -5.36 |
| <i>Mp1g29040</i> | Aquaporin         | -4.75 | -3.03 |
| <i>Mp2g22780</i> | Chalcone synthase | -5.50 | -6.98 |



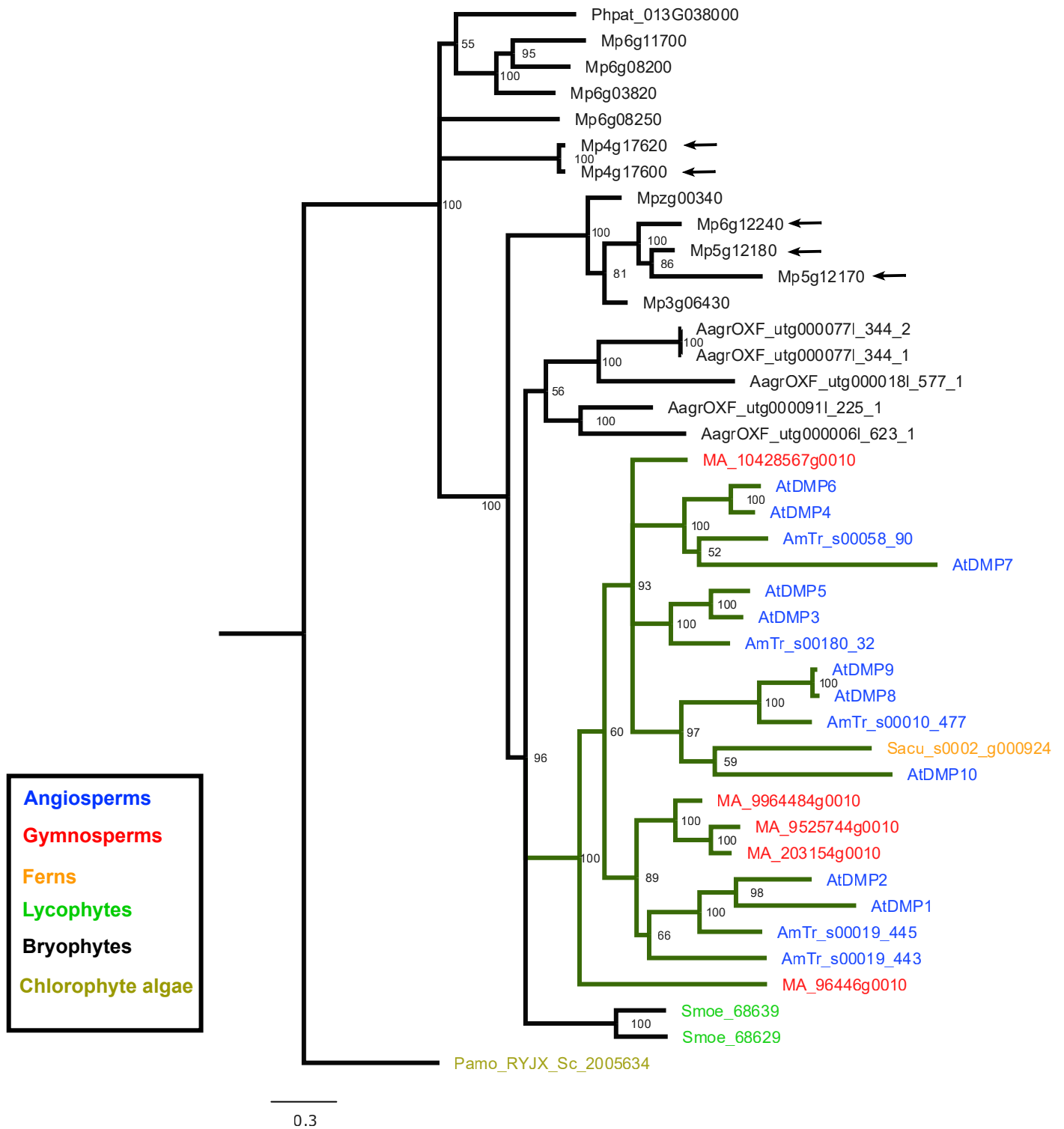
**(A) VND proteins phylogeny.** Bayesian phylogeny, rooted on the streptophyte algal accession SM000175S03281. A well supported clade containing the Arabidopsis VND proteins is highlighted in green, this also contains the single Marchantia orthologue MpNAC5 as well as the moss VND proteins numbered as in the Xu et al 2014 characterization. The species abbreviations are SM *Spirogloea musicola*, ME *Mesotaenium endlicherianum*, Smoe *Selaginella moellendorffii*, Sacu *Salvinia cucullata*, At *Arabidopsis thaliana*, Amtr *Amborella trichopoda*, Apun *Anthoceros punctatus*, Mp *Marchantia polymorpha*, Phpat *Physcomitrium patens*, MA *Picea abies*. Species are coloured according to major taxonomic groupings as indicated in legend on left.



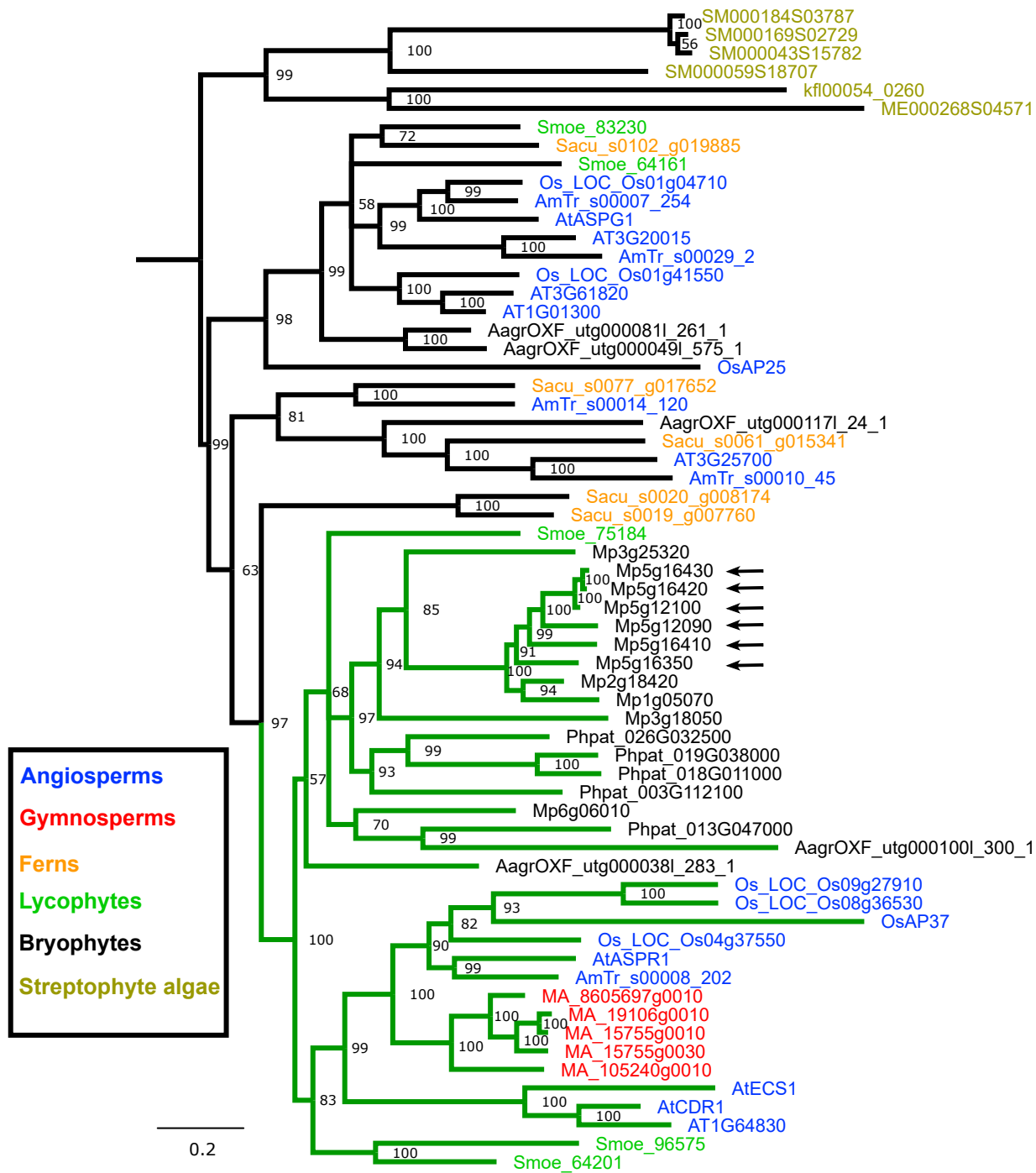


0.2

**(B) Metacaspase phylogeny.** Bayesian phylogeny, midpoint rooted, with posterior probabilities indicated at nodes. A well supported clade containing the type II metacaspases is indicated in red. MpMCA-IIc identified in the RNA seq experiment is highlighted with a blue arrow and is clearly a type II metacaspase and is equally related to the five Arabidopsis type II metacaspases. The species abbreviations are Cre *Chlamydomonas reinhardtii*, Spmu *Spirogloea musicola*, Smoe *Selaginella moellendorfii*, Sacu *Salvinia cucullata*, Nt *Nymphaea thermarum*, At *Arabidopsis thaliana*, Amtr *Amborella trichopoda*, Aagr *Anthoceros agrestis*, Mp *Marchantia polymorpha*, Phpat *Physcomitrium patens*, MA *Picea abies*. Species are coloured according to major taxonomic groupings as indicated in legend on left.



**(C) DMP-like protein phylogeny.** Bayesian phylogeny, rooted on Pamo\_RYJX\_Sc\_2005634. The five *Marchantia* DMP-like genes identified in the RNA-seq experiment are highlighted with arrows. The ten *Arabidopsis* DMP-like genes and the *Marchantia* genes diversified after the bryophyte/tracheophyte split. The species abbreviations are Pamo *Pandorina morum*, Smoe *Selaginella moellendorffii*, Sacu *Salvinia cucullata*, Nt *Nymphaea thermarum*, At *Arabidopsis thaliana*, Amtr *Amborella trichopoda*, Agr *Anthoceros agrestis*, Mp *Marchantia polymorpha*, Phpat *Physcomitrium patens*, MA *Picea abies*. Species are coloured according to major taxonomic groupings as indicated in legend on left.



**(D) Aspartic protease phylogeny.** Bayesian phylogeny, midpoint rooted, with posterior probabilities indicated at nodes. A well supported clade containing the rice OsAP37 aspartic protease, implicated in tapetal dPCD, is highlighted in green. The five *Marchantia* aspartic proteases that were identified as down regulated in *Mpzou1* and *Mpice1* mutants are indicated with arrows. The species abbreviations are SM *Spirogloea musicola*, Kfl *Klebsormidium nitens*, ME *Mesotaenium endlicherianum*, Smoe *Selaginella moellendorffii*, Sacu *Salvinia cucullata*, Os *Oryza sativa*, At *Arabidopsis thaliana*, Amtr *Amborella trichopoda*, Agr *Anthoceros agrestis*, Mp *Marchantia polymorpha*, Phpat *Physcomitrium patens*, MA *Picea abies*. Species are coloured according to major taxonomic groupings as indicated in legend on left.